PI(3,5)P_2 controls endosomal branched actin dynamics by regulating cortactin–actin interactions

Nan Hyung Hong,[1] Aidong Qi,[2] and Alissa M. Weaver[1,3,4]

[1]Department of Cancer Biology, [2]Department of Biochemistry, [3]Department of Cell and Developmental Biology, and [4]Department of Pathology, Microbiology, and Immunology, Vanderbilt University Medical Center, Nashville, TN 37232

Branched actin critically contributes to membrane trafficking by regulating membrane curvature, dynamics, fission, and transport. However, how actin dynamics are controlled at membranes is poorly understood. Here, we identify the branched actin regulator cortactin as a direct binding partner of phosphatidylinositol 3,5-bisphosphate (PI(3,5)P_2) and demonstrate that their interaction promotes turnover of late endosomal actin. In vitro biochemical studies indicated that cortactin binds PI(3,5)P_2 via its actin filament-binding region. Furthermore, PI(3,5)P_2 competed with actin filaments for binding to cortactin, thereby antagonizing cortactin activity. These findings suggest that PI(3,5)P_2 formation on endosomes may remove cortactin from endosome-associated branched actin. Indeed, inhibition of PI(3,5)P_2 production led to cortactin accumulation and actin stabilization on Rab7$^+$ endosomes. Conversely, inhibition of Arp2/3 complex activity greatly reduced cortactin localization to late endosomes. Knockdown of cortactin reversed PI(3,5)P_2-inhibitor–induced actin accumulation and stabilization on endosomes. These data suggest a model in which PI(3,5)P_2 binding removes cortactin from late endosomal branched actin networks and thereby promotes net actin turnover.

Introduction

Dynamic branched actin assembly occurs at cellular membranes and is nucleated by the Arp2/3 complex upon activation by a member of the Wiskott-Aldrich Syndrome protein (WASP) family (Goley and Welch, 2006). Diverse WASP family members are recruited to distinct cellular membranes by membrane-associated signaling complexes that function as localization and activation factors. A contributing factor to dynamic actin assembly is the molecule cortactin, which localizes to all sites of branched actin assembly and both promotes WASP-induced actin polymerization and stabilizes actin branches after their formation (Uruno et al., 2001; Weaver et al., 2001, 2002; Goley and Welch, 2006). Most branched actin assemblies have lifetimes in the seconds-to-minutes timescale and are much more dynamic than other forms of cellular actin (Lai et al., 2008; Puthenveedu et al., 2010). The dynamic nature of branched actin is likely critical for its functions in controlling dynamic protrusions and other membrane-based events.

Increasing evidence indicates that actin plays an important role in postinternalization events along the endocytic pathway, including endosomal tubulation, vesicle fusion, and fission, and endosome motility (Derivery et al., 2009; Duleh and Welch, 2010; Puthenveedu et al., 2010; Ohashi et al., 2011; Tanabe et al., 2011; Monteiro et al., 2013). Consistent with its integral role in Arp2/3 complex–mediated branched actin assembly, cortactin has been shown to regulate many of these processes. Our previous studies showed that cortactin controls late endosomal/lysosomal maturation and subsequent retrograde transport to the Golgi apparatus (Kirkbride et al., 2012). In addition, cortactin regulation of dynamic actin assembly on endosomes in coordination with Arp2/3 complex and Wiskott-Aldrich syndrome protein and Scar homologue (WASH) was shown to control cargo sorting (Puthenveedu et al., 2010; Ohashi et al., 2011; Monteiro et al., 2013). Furthermore, cortactin promotes actin-mediated fusion of autophagosomes with lysosomes (Lee et al., 2010). Collectively, these data indicate that cortactin is a key regulator of actin-dependent endosomal processes. However, how cortactin itself is controlled on endosomes is poorly understood.

Phosphoinositides (PIs) are membrane phospholipids that are generated in small amounts at specific cellular membranes by distinct PI kinases. PIs decorate a given organelle with molecular identity and recruit specific effector proteins to confer a distinct set of functions (Behnia and Munro, 2005; Di Paolo and De Camilli, 2006; Kutateladze, 2010), including regulation of the actin cytoskeleton (Janmey and Lindberg, 2004; Saarikangas et al., 2010). Among different PIs, PI4,5-bisphosphate (PI(4,5)P_2) is the best-characterized regulator of actin organization. PI(4,5)P_2 binding to N-WASP is a key step in N-WASP activation by inducing a conformational change that releases the Arp2/3-binding VCA domain (Rohatgi et al., 2000; Pa-

Correspondence to Alissa M. Weaver: alissa.weaver@vanderbilt.edu

Abbreviations used in this paper: KD, knockdown; PI(3,5)P_2, phosphatidylinositol 3,5-bisphosphate; TIRF, total internal reflection fluorescence; WASH, Wiskott-Aldrich Scar homologue; WASP, Wiskott-Aldrich Syndrome protein.

The Rockefeller University Press $30.00
J. Cell Biol. Vol. 210 No. 5 753–769
www.jcb.org/cgi/doi/10.1083/jcb.201412127

payannopoulos et al., 2005). PI(4,5)P_2 also controls actin filament severing, capping, cross-linking, and actin–membrane binding interactions, through interactions with actin-binding proteins such as cofilin, gelsolin, capZ, filamin, α-actinin, vinculin, and talin (Yin and Janmey, 2003; Janmey and Lindberg, 2004). In addition, PI(3,4,5)P_3 regulates activation of the WASP family member WAVE2 to control lamellipodial protrusion (Suetsugu et al., 2006). However, because PI(4,5)P_2 and PI(3,4,5)P_3 primarily mark the plasma membrane, the role of PIs in controlling actin dynamics at other membrane compartments is less well understood.

PI(3,5)P_2 is a low-abundance PI that mainly localizes to late endosomes and lysosomes in higher eukaryotes (Ikonomov et al., 2006; Michell et al., 2006) and in the yeast vacuole (Rudge et al., 2004). PI(3,5)P_2 directs trafficking of cargo vesicles along the endosome–lysosome axis, and governs a plethora of associated cellular functions, including endolysosome morphology, acidification, autophagy, stress-induced signaling, and ion channel activity (Yin and Janmey, 2003; Shisheva, 2008; de Lartigue et al., 2009; Dove et al., 2009). Defects in the regulation of PI(3,5)P_2 are linked to several human diseases, including Charcot-Marie-Tooth type 4 and amyotrophic lateral sclerosis, which are thought to be caused by defective autophagy (Bolino et al., 2000; Chow et al., 2007; Ferguson et al., 2009; Kotoulas et al., 2011; Otomo et al., 2012). Despite the well-characterized roles of PI(3,5)P_2 in endolysosomal trafficking and disease, few molecular effector proteins of PI(3,5)P_2 have been identified.

In this study, we characterize a novel and direct binding interaction of cortactin with PI(3,5)P_2. We show that purified cortactin interacts with PI(3,5)P_2 through its filamentous actin (F-actin) binding domain. Furthermore, PI(3,5)P_2 competes with F-actin for binding to cortactin, leading to inhibition of cortactin-mediated branched actin nucleation and stabilization. Inhibition of PI(3,5)P_2 synthesis in cells resulted in actin stabilization on late endosomes which is abolished by cortactin depletion. Based on these findings, we propose a model in which PI(3,5)P_2 removes cortactin from nascent membrane-associated actin, limiting overall assembly of branched actin at late endosomes. Cycles of conversion between PI(3)P and PI(3,5)P_2 may allow fast actin dynamics on endosomal membranes and consequent membrane-trafficking events.

Results

Cortactin directly binds to PI(3,5)P_2

Cortactin regulates branched actin assembly at membranes throughout the cell. Because cortactin has a putative PI-binding site in its N terminus (He et al., 1998), we hypothesized that PIs might regulate its recruitment or activity at specific membrane sites. To test this hypothesis and identify candidate PI binding partners, we performed a lipid overlay assay with GST-tagged full-length cortactin. GST-fusion proteins (Fig. S1 A, Coomassie staining) were incubated with phospholipids immobilized on a nitrocellulose membrane (PIP strip). Full-length cortactin interacted most strongly with PI(3,5)P_2 (Fig. 1 A), and to a much lesser extent with other phosphoinositides, including PI(3)P and PI(5)P. Hrs-FYVE and PLC-PH lipid-binding domains were used as respective positive controls for PI(3)P and PI(4,5)P_2 binding.

PI(3,5)P_2 is found with highest abundance on late endosomes (Di Paolo and De Camilli, 2006; Michell et al., 2006), where cortactin also has been shown to localize (Sung et al., 2011; Kirkbride et al., 2012; Rossé et al., 2014). To further validate the interaction and determine whether cortactin interacts directly with PI(3,5)P_2 in more physiologically relevant conditions, we performed a liposome pull-down assay. Commercial PolyPIPosome liposomes containing 5% PI (PI(3,5)P_2, PI(3)P, or PI(5)P) and 1% biotin-phosphatidylethanolamine in a mixture of phosphatidylcholine and phosphatidylethanolamine were incubated with GST–cortactin, and then isolated with streptavidin-coated magnetic beads. GST alone and the PI(3)P-binding protein GST-2xFYVE were used as respective negative and positive controls. Western blot analysis of the pull-downs revealed that full-length cortactin specifically binds liposomes containing PI(3,5)P_2, but not PI(3)P or PI(5)P (Fig. 1, B and C, probed with anti-GST antibody; Fig. S1 C, probed with anti-cortactin antibody). Analysis of binding isotherms with varying lipid input revealed an apparent equilibrium dissociation constant (K_d) of 30 nM for cortactin–PI(3,5)P_2 interactions (Fig. 1 D). Collectively, these results indicate that cortactin directly and specifically binds to PI(3,5)P_2.

Inhibition of PI(3,5)P_2 synthesis leads to accumulation of cortactin on late endosomes

The enzyme complex that synthesizes PI(3,5)P_2 localizes to both early and late endosomes and consists of the scaffold protein Vac14, the lipid kinase PIKfyve (which converts PI(3)P to PI(3,5)P_2), and the counteracting lipid phosphatase Fig4 (Rudge et al., 2004; Ikonomov et al., 2006; Nicot et al., 2006; Rusten et al., 2006; Rutherford et al., 2006). To determine whether cortactin and the PI(3,5)P_2-synthesizing enzyme complex are likely to be present in the same compartment, we immunolocalized cortactin with Vac14. Immunostaining of SCC61 and HeLa cells transiently expressing hVac14-EGFP (Jin et al., 2008) with antibodies against cortactin revealed that cortactin is indeed present on Vac14$^+$ vesicular structures (Fig. 2 A). To further determine whether cortactin is present at PI(3,5)P_2-containing endosomes, we localized cortactin with a specific probe for PI(3,5)P_2, mCherry-ML1N*2 (Li et al., 2013), and with the late endosomal marker Rab7. As expected, mCherry-ML1N*2 and Rab7 were present together in the same endosomal populations with virtually all ML1N*7$^+$ endosomes containing Rab7$^+$ puncta or rings (Fig. 2, B and C). Consistent with the role of PI(3,5)P_2 in late endosomal maturation (de Lartigue et al., 2009; Dove et al., 2009), individual endosomes had different proportions of Rab7 or ML1N*2 positivity (Fig. 2 C). Cortactin localized to some of these Rab7-ML1N*2$^+$ endosomes (Fig. 2 B).

A central function of PIs on membranes is recruitment of cytosolic proteins, including cytoskeletal proteins (Janmey and Lindberg, 2004). To investigate whether PI(3,5)P_2 recruits cortactin to endosomes, we prevented cellular PI(3,5)P_2 synthesis by knocking down PIKfyve expression with siRNA in MDA-MB-231 cancer cells (Fig. 2 D). Consistent with previous studies, inhibition of PIKfyve led to enlargement of late endosomes marked by Rab7 (Fig. 2 E; Nicot et al., 2006). Surprisingly, silencing of PIKfyve led to a marked increase in cortactin localization to Rab7$^+$ late endosomes rather than the expected decrease (Fig. 2, E and F). Likewise, treatment of MDA-MB-231 or SCC61 cells with the specific PIKfyve inhibitor drugs YM201636 (Ikonomov et al., 2006; Jefferies et al., 2008; de Lartigue et al., 2009) or apilimod (Cai et al.,

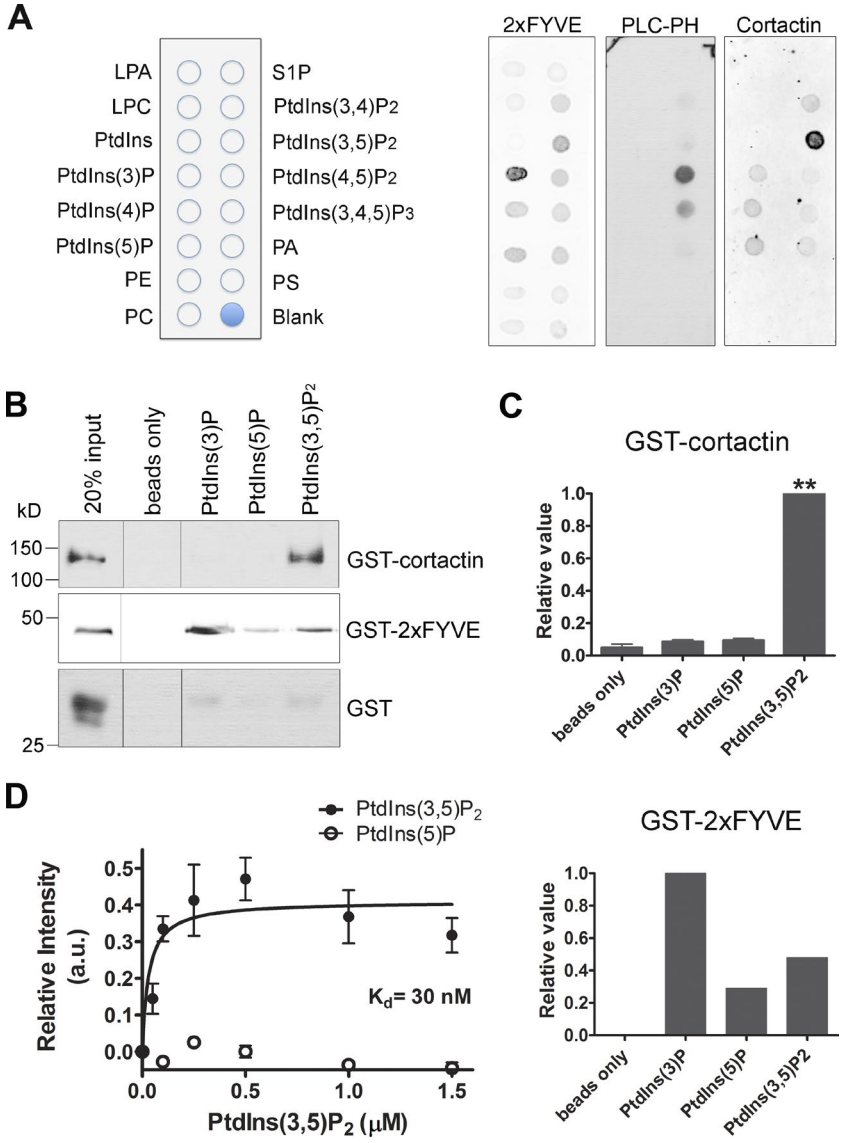

Figure 1. **Cortactin directly interacts with PI(3,5)P_2.** (A) The affinity of full-length cortactin was examined using a protein-lipid overlay assay. The left panel indicates the identity of lipid species on the PIP strip. Cortactin binds most strongly to PI(3,5)P_2. Binding of the FYVE domain of Hrs (2xFYVE) and PH domain of PLC-δ1 to PI(3)P and PI(4,5)P_2, respectively, served as positive controls. (B) Pull-down of GST–cortactin by liposomes bearing the indicated PIPs. GST-2xFYVE, and GST alone are respectively positive and negative controls. Western blots were probed with anti-GST antibody. (C) The relative binding of GST-fusion proteins to liposomes containing different PIPs was quantified by densitometric analysis of GST immunoblots from three independent experiments, except for positive control GST-2xFYVE that was tested once for pull-down by PI(3)P. Mean ± SE. **, $P < 0.01$. (D) Cortactin binding PI(3,5)P_2- or PI(5)P-containing liposomes, plotted as a function of PIP concentration. Data points in the PI(3,5)P_2 and negative control PI(5)P binding curves represent means calculated from data points of five and two different experiments, respectively. The K_d for cortactin–PI(3,5)P_2 interaction obtained from nonlinear regression of the data are 30 nM.

2013) phenocopied the effect of PIKfyve siRNA (Fig. 3, A and C; Fig. S2, A–D; and Video 1). Despite inducing enlargement of individual endosomes, YM201636 drug treatment had no significant effect on the total Rab7$^+$ endosome area per cell (Fig. 3 E), suggesting that the increased overlap between cortactin and Rab7$^+$ area per cell (Fig. 3 C) is not a secondary effect of endosomal enlargement. Immunofluorescence of YM201636-treated cells using early (EEA1) and late endosomal (Rab7) markers confirmed that the majority of the enlarged vesicular compartments were Rab7$^+$ with only a few endosomes positive for both EEA1 and Rab7, reflecting perturbation in late endosomal maturation and/or trafficking (Fig. S2 E; Rutherford et al., 2006). These data indicate that PI(3,5)P_2 does not function to recruit cortactin to late endosomes but may instead regulate its activity by removing it from the late endosome.

Inhibition of PI(3,5)P_2 synthesis leads to cortactin-dependent actin accumulation on Rab7$^+$ endosomes

Cortactin has a unique role as a regulator of Arp2/3 complex by promoting both assembly and stability of branched actin networks (Uruno et al., 2001; Weaver et al., 2001). Along with cortactin, inhibition of PI(3,5)P_2 synthesis by MDA-MB-231 and SCC61 cells with YM201636, apilimod, or knockdown (KD) of PIKfyve caused a striking enrichment of actin on Rab7$^+$ endosomes (Fig. 2 E; Fig. 3 A; and Fig. S2 C). Quantitative analysis of the imaging data demonstrated that actin intensity and the number of actin dots on Rab7$^+$ endosomes were significantly increased in YM201636-treated cells (Fig. 3, F and G). Colocalization of actin with Rab7 was also increased in YM201636- and apilimod-treated and PIKfyve-KD cells (Fig. 2 F; Fig. 3 D; Fig. S2 B [compare YM201636 and DMSO treatments in control cells]; and Fig. S2 D). The YM201636-induced accumulation of actin on late endosomes was reversed in cortactin–KD cells (Fig. 3 D and Fig. S2 B). These data indicate that PI(3,5)P_2 synthesis on late endosomes attenuates actin accumulation. Furthermore, in the absence of PI(3,5)P_2, actin accumulates in a cortactin-dependent manner.

Cortactin localization to late endosomes depends on Arp2/3 complex activity

One mechanism by which cortactin could promote accumulation of actin on endosomes is by regulating branched actin

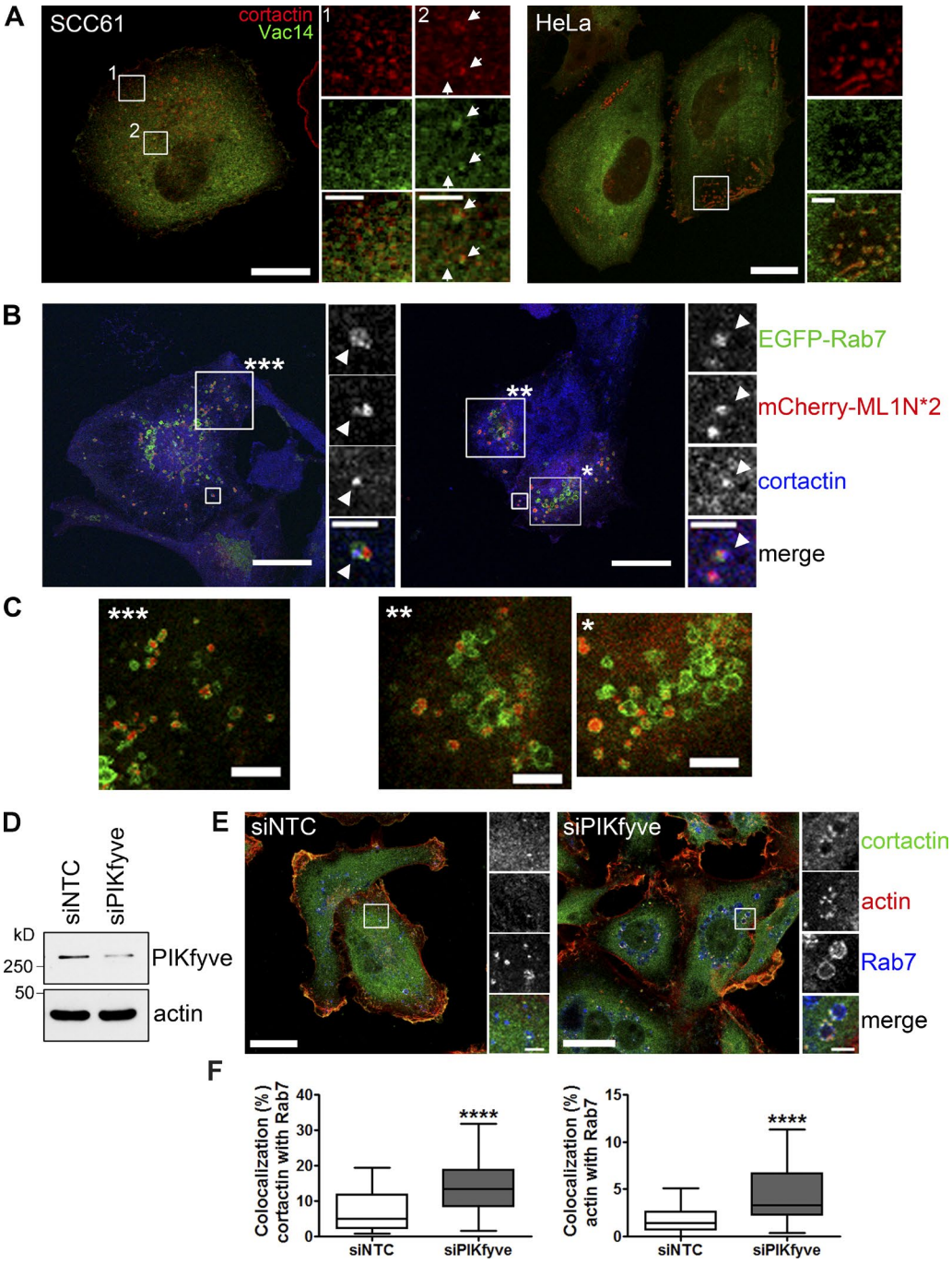

Figure 2. **KD of PIKfyve expression leads to accumulation of cortactin and actin at LE membrane.** (A) Representative images of endogenous cortactin (red) localized at discrete subdomains of hVac14-EGFP+ (green) vesicular structures in SCC61 (left) and HeLa (right) cells. Bars: (main panels) 20 µm; (enlarged views) 3 µm. $n = 3$ independent experiments for each cell line. (B) Representative images of mCherry-ML1N*2 (red) and endogenous cortactin (blue) localization to EGFP-Rab7+ (green) endosomes. Small white boxes are enlarged on the right. Bars, 20 µm (3 µm for magnifications). (C) Magnifications of boxed areas labeled with asterisks in B show colocalization of mCherry-ML1N*2 (red) with EGFP-Rab7 (green). Bars, 5 µm. (D) Immunoblot of PIKfyve expression in PIKfyve-KD MDA-MB-231 cells. NTC, nontargeting control. (E) Immunofluorescence of PIKfyve siRNA-treated cells using antibodies recognizing cortactin (green), actin (red), and Rab7 (blue). Bars, 20 µm (3 µm for magnifications). (F) Percentage of colocalization of cortactin or actin with Rab7. 3 independent experiments, $n \geq 61$ cells in each condition. ****, $P < 0.0001$.

network assembly by the Arp2/3 complex (Uruno et al., 2001; Weaver et al., 2001). To determine whether Arp2/3-mediated branched actin nucleation is required for recruiting cortactin to endosomal membranes, we treated cells with the Arp2/3 complex inhibitor CK-666 (Nolen et al., 2009; Hetrick et al., 2013). Treatment with CK-666 resulted in significantly reduced cortactin localization on Rab7+ endosomes (Fig. 4, A and B). Moreover, the accumulation of cortactin that occurs with inhibition of $PI(3,5)P_2$ synthesis by YM201636 was abolished in CK-666–treated cells. Like-

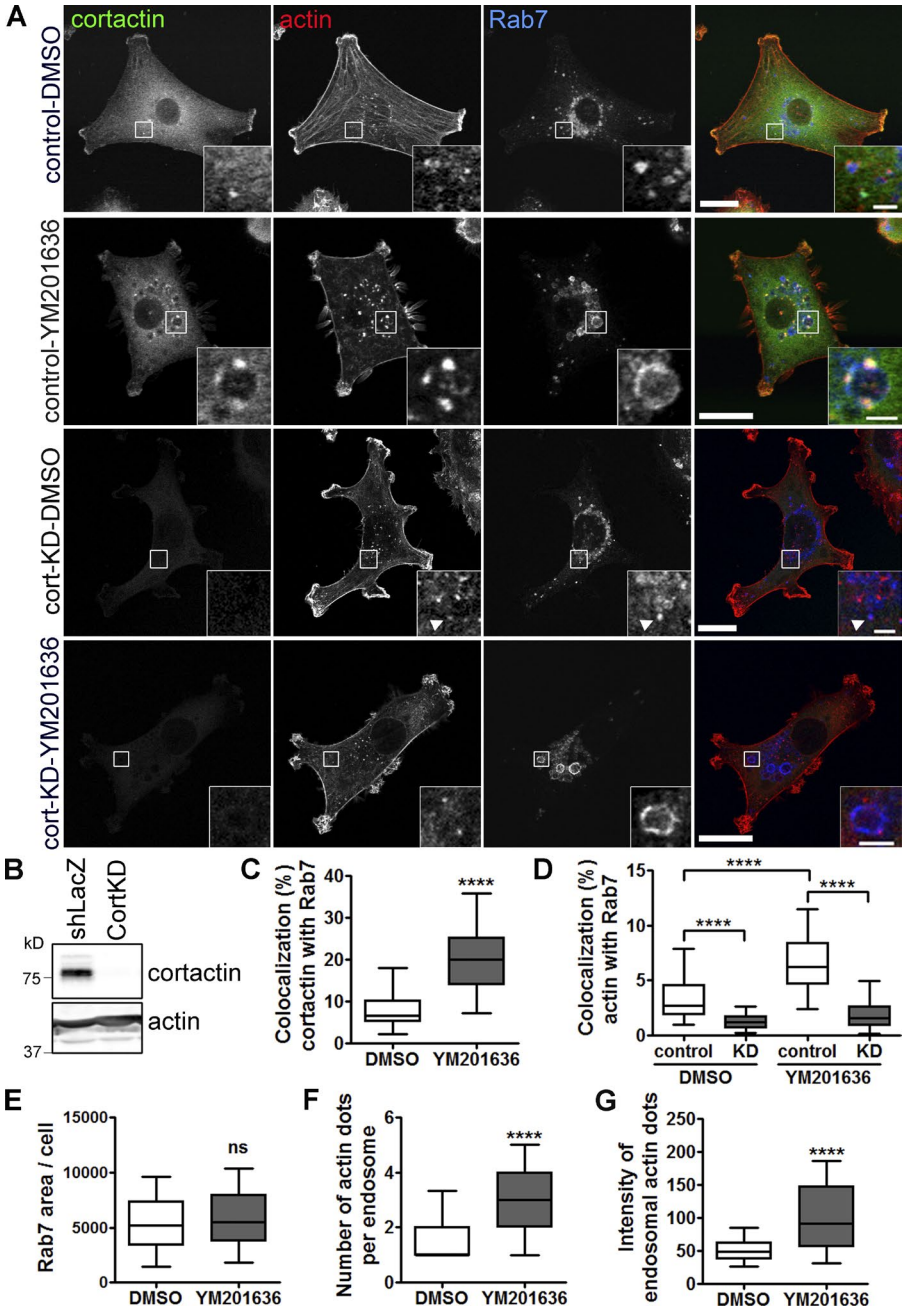

Figure 3. **Inhibition of PI(3,5)P_2 production leads to accumulation of cortactin and actin at LE membrane.** (A) Representative images showing cortactin (green) and actin (red) localization on Rab7$^+$ endosomes (blue) after 2-h treatment with 800 nM YM201636 or DMSO diluent control in control and cortactin–KD MDA-MB-231 cells. Bars, 20 µm (3 µm for magnifications). (B) Immunoblot of cortactin expression and β-actin loading control in MDA-MB-231 cells. (C–E) Images were analyzed for percentage of colocalization of cortactin or actin with Rab7 or Rab7 area per cell. 3 independent experiments, $n \geq 55$ cells in each condition. (F and G) Number and intensity of actin dots on Rab7$^+$ endosomes. More than 170 vesicles from 12–19 cells analyzed for each condition. Data shown as box and whiskers plots, with the box indicating the 25th and 75th percentiles, solid line indicating the median, and whiskers indicating the 95% confidence intervals. ****, $P < 0.0001$.

wise, Arp2/3 inhibition with CK-666 treatment inhibited actin accumulation on Rab7$^+$ late endosomes in both control and YM201636-treated cells (Fig. 4, A and C). These data suggest a model in which cortactin is recruited to late endosomes by interactions with branched actin networks and removed by interaction with PI(3,5)P_2.

The fourth repeat region of cortactin is necessary for PI(3,5)P_2 binding

Cortactin does not contain canonical phosphoinositide-binding motifs, such as PH (pleckstin homology) or FYVE domains. However, it has been predicted that a series of basic lysine residues within the N-terminal fourth repeat domain of cortactin may bind phosphoinositides (He et al., 1998). The fourth repeat region of cortactin is also thought to be a critical F-actin–binding site (Weed et al., 2000) and binding to F-actin is required for cortactin to regulate Arp2/3-mediated branched actin assembly and stability (Uruno et al., 2001; Weaver et al., 2001). Thus, binding of PI(3,5)P_2 to this region could modulate the interaction of cortactin with actin filaments.

To map the PI(3,5)P_2 binding site of cortactin, we tested the ability of the purified cortactin N terminus and fourth repeat deletion mutant to bind PI(3,5)P_2-containing liposomes (Fig. 5 A). The cortactin repeat domains each contain 37 aa (Wu et al., 1991) and are not likely to be involved in large scale folding of cortactin because common splice variants of cortactin have lost either the sixth or fifth + sixth repeats (van Rossum et al., 2003) and purified cortactin has been shown to have an extended structure (Weaver et al., 2002). Furthermore, deletion of the fourth repeat domain from either end of N- or C-terminal cortactin fragments leads to loss of binding of those fragments to actin filaments (Weed et al., 2000), suggesting a specific activity

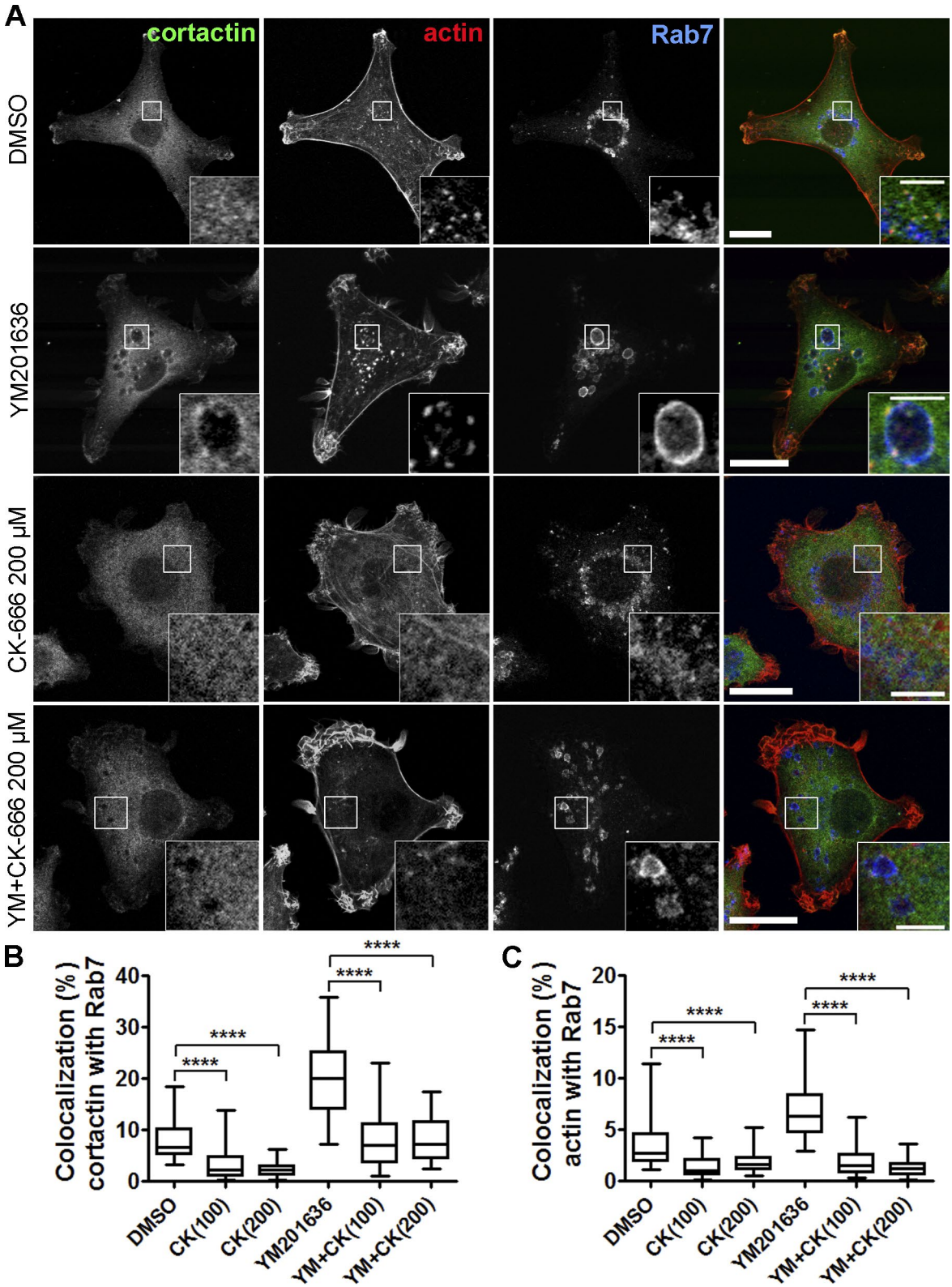

Figure 4. **Recruitment of cortactin to late endosomes depends on Arp2/3 complex activity.** (A) Representative images show cortactin (green), actin (red), and Rab7 (blue) localization after 2 h treatment of MDA-MB-231 cells with 800 nM YM201636 ± 200 µM CK-666. Bars, 20 µm (5 µm for magnifications). (B) Images from cells treated with YM201636 and 100 or 200 µM CK-666 were analyzed for percentage of colocalization of cortactin or actin with Rab7. The DMSO and YM201636 datasets (no CK-666) are the same data as that shown in Fig. 3 (C and D). Data shown as box and whiskers plots with the box indicating the 25th and 75th percentiles, solid line indicating the median, and whiskers indicating the 95% confidence intervals. 3 independent experiments, $n \geq 50$ cells for each condition. ****, $P < 0.0001$.

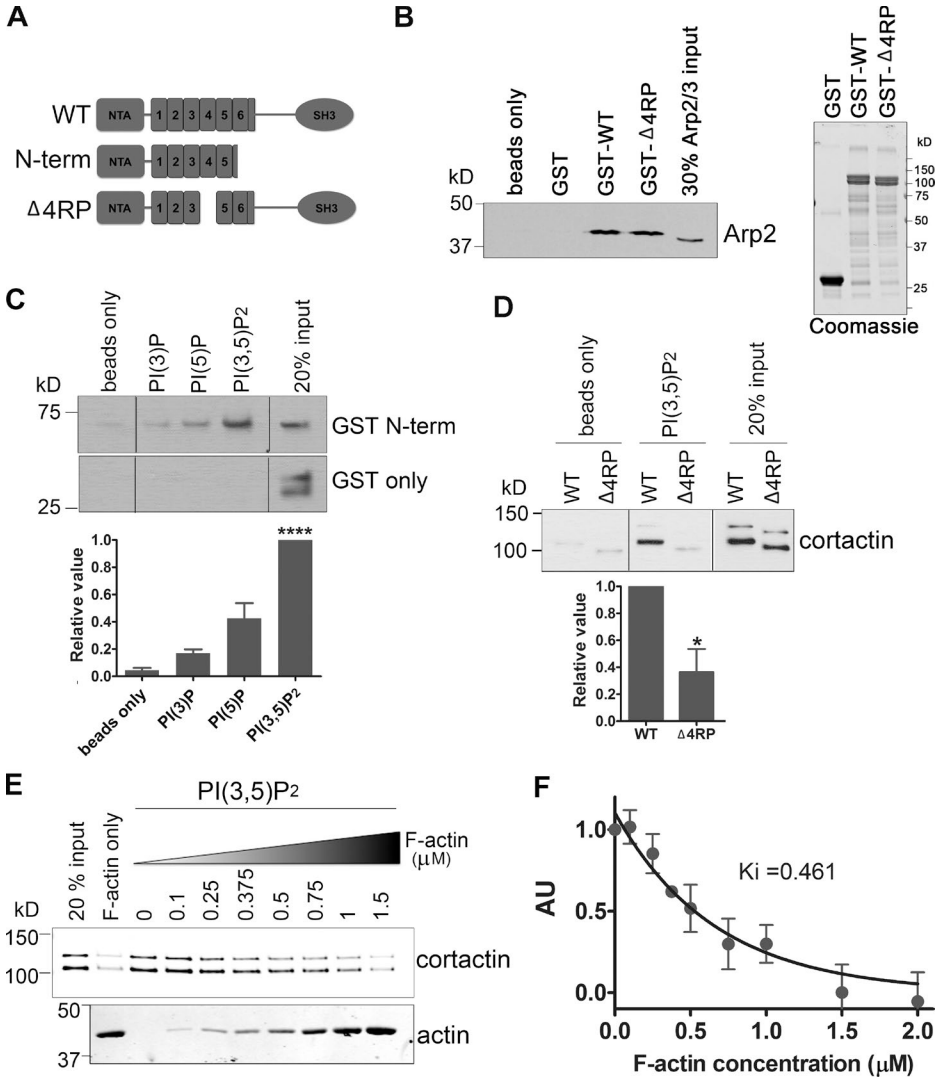

Figure 5. **PI(3,5)P_2 regulates the interaction of cortactin with actin filaments.** (A) Schematic of WT and mutant cortactin constructs. (B, left) Representative Western blot from n = 3 Arp2/3 binding experiments, probed with an antibody to Arp2. (right) Coomassie-stained gel of GST-tagged proteins immobilized on glutathione beads used in Arp2/3 binding experiment. The same amount of beads was loaded in each lane and used in the experiment. (C and D) Representative Western blots from (C) GST-N-term and (D) GST-Δ4RP cortactin–pull-down experiments. Cortactin proteins bound to PI(3,5)P_2-liposomes were identified with an anti-GST antibody. Relative binding affinity was quantified by densitometric analysis of Western blot data from three independent experiments. Mean ± SE. *, $P < 0.05$; ****, $P < 0.0001$. (E and F) F-actin competes with PI(3,5)P_2 for binding to cortactin. (E) Increasing concentrations of actin filaments were incubated with 70 nM cortactin and 250 nM PI(3,5)P_2-containing liposomes. In the presence of F-actin, cortactin binding to liposomes was significantly reduced. (F) Data points show mean binding from four independent experiments. Fit to hyperbolic decay model yields a K_i value of 0.461 μM.

of that domain and not whole-scale unfolding of the molecule. Finally, we find that cortactin lacking the fourth repeat can still bind to Arp2/3 complex (Fig. 5 B), further suggesting that loss of the fourth repeat domain does not affect cortactin activities located in other parts of the N terminus. Consistent with our hypothesis that the PI(3,5)P_2 binding activity might be located in the fourth repeat domain in the N terminus, we found that the N terminus of cortactin is sufficient to bind PI(3,5)P_2 (Fig. 5 C), whereas the fourth repeat deletion mutant of cortactin cannot bind PI(3,5)P_2-liposomes (Fig. 5 D).

To further delineate the role of the fourth repeat in binding F-actin and PI(3,5)P_2, we made a series of charge-neutralizing mutations that changed lysines present in the fourth repeat to glutamine (Fig. S3, A and B: 1Q, 2Q, 3Q, 5Q, and 8Q mutants). Analysis of the purified proteins in an actin co-sedimentation assay revealed that the ability of cortactin to bind to actin filaments was progressively lost with increasing numbers of mutated lysines (Fig. S3 C). There was also a trend toward decreased binding of the mutants to PI(3,5)P_2. However, only the 8Q mutant exhibited significantly lower specific binding to PI(3,5)P_2, potentially because of variability associated with increased nonspecific binding of the mutant proteins to the beads used for the pull-down assays (Fig. S3 D, beads only lanes in blots).

PI(3,5)P_2 competes with actin filaments for binding to cortactin

Altogether, our binding data with the N terminus, fourth repeat mutant, and 1Q-8Q mutants suggest that actin filaments and PI(3,5)P_2 both bind to sites in the fourth cortactin repeat which could be overlapping. To specifically test the hypothesis that PI(3,5)P_2 competes with actin filaments for binding to cortactin, we performed in vitro binding assays using purified proteins. As shown in Fig. 5 (E and F) the addition of increasing concentrations of actin filaments to samples containing cortactin and PI(3,5)P_2-liposomes led to a dose-dependent decrease in the amount of cortactin bound to the liposomes. The Ki of 0.461 μM is consistent with the lower published affinity of cortactin for F-actin (K_d = 0.250 μM, (Bryce et al., 2005)) than for PI(3,5)P_2 (K_d = 30 nM, Fig. 1).

PI(3,5)P_2 affects in vitro activity of cortactin

The finding that PI(3,5)P_2 prevents cortactin from binding to actin filaments suggests that PI(3,5)P_2 may inhibit the activity of cortactin in controlling branched actin dynamics. To directly test the role of cortactin in branched actin nucleation, we used total internal reflection fluorescence (TIRF) microscopy to monitor formation of branched actin filaments from purified proteins

in real time (Videos 2, 3, 4, 5, and 6). Consistent with previous studies (Weaver et al., 2001, 2002; Uruno et al., 2003; Siton et al., 2011; Helgeson and Nolen, 2013; Helgeson et al., 2014), addition of cortactin to reactions containing Arp2/3 complex, the active VCA domain of N-WASp (GST-VCA), and G-actin increased the rate of actin branch formation (Fig. 6, A and B). Addition of 200 nM PI(3,5)P_2-liposomes significantly reduced cortactin-induced enhancement of branched actin assembly, although it did not totally ablate it. At higher concentrations of liposomes there was a greater inhibition of cortactin-mediated enhanced branched actin assembly; however there was also an effect on control reactions (unpublished data). In contrast, at concentrations ≤200 nM, PI(3,5)P_2-liposomes had no effect on branching induced by GST-VCA+Arp2/3 complex in the absence of cortactin, indicating a selective effect on cortactin. Addition of 200 nM PI(3,4)P_2-liposomes had no effect on cortactin-regulated branching (Fig. 6, A and B), consistent with the minimal binding of cortactin to PI(3,4)P_2 detected in the PIP strip assay (Fig. 1 A) and suggesting a specific effect of PI(3,5)P_2. Because cortactin is also known to stabilize actin branches (Weaver et al., 2001), we tested whether PI(3,5)P_2 prevents branch stabilization by cortactin. Actin filaments were prepolymerized in the presence of Arp2/3 complex and GST-VCA and then cortactin, PI(3,5)P_2-liposomes, both cortactin and PI(3,5)P_2-liposomes, both cortactin and PI(3,4)P_2-liposomes, or buffer were added to individual reactions. For the debranching assay, 500 nM PI(3,5)P_2-liposomes had no effect on control reactions so the higher concentration was used. At various time points, rhodamine-phalloidin was added to visualize and stabilize the filaments and images were obtained. The number of branched actin filaments at each time point was quantitated. Consistent with previous observations (Weaver et al., 2001), the presence of cortactin inhibited debranching (Fig. 6, C and D). In contrast, the addition of PI(3,5)P_2-liposomes but not PI(3,4)P_2-liposomes reversed branch stabilization by cortactin but had no effect on control networks (Fig. 6, C and D). Together, these data indicate that PI(3,5)P_2 can remodel branched actin networks by regulating the interaction of cortactin with actin filaments.

PI(3,5)P_2 regulates actin stability on late endosomes

The finding that PI(3,5)P_2 competes with F-actin for binding to cortactin (Fig. 5, E and F) suggests that synthesis of PI(3,5)P_2 may regulate cortactin cycling on and off of branched actin networks on late endosomal membranes. Consistent with that model, we found that inhibition of PI(3,5)P_2 synthesis leads to accumulation of cortactin on Rab7$^+$ endosomes (Fig. 2, D–F; Fig. 3; and Fig. S2, A–D). In addition, PI(3,5)P_2-mediated removal of cortactin from actin branchpoints could lead to decreased actin assembly and/or destabilization of branched actin networks associated with the endosomal surface. Indeed, in fixed cell analyses, we found that inhibition of PI(3,5)P_2 synthesis led to cortactin-dependent accumulation of actin on Rab7$^+$ endosomes (Fig. 3 and Fig. S2, A and B). To test whether endosomal actin turnover is regulated by cortactin and PI(3,5)P_2, live imaging was performed on control or cortactin–KD cells expressing the dynamic actin probe mGFP-F-tractin in the presence or absence of the PI(3,5)P_2 synthesis inhibitor YM201636. To specifically analyze actin turnover, cells were treated with 10 µM latrunculin A, a drug that prevents actin polymerization by sequestering monomeric actin (Morton et al., 2000). In control cells treated with DMSO as the diluent control for YM201636, endosomal actin fluorescence became undetectable within 40–50 s after Latrunculin A. A quantitative analysis across multiple control cells revealed an exponential loss in the intensity of endosomal actin fluorescence after latrunculin exposure, with a $t_{1/2}$ of 20.8 s. In contrast, endosomal actin fluorescence in YM201636-treated cells decreased more slowly, yielding a $t_{1/2}$ of 109.3 s. (Fig. 7 and Video 7), indicating that PI(3,5)P_2 is important for dynamic turnover of late endosomal actin assemblies. DMSO-treated cortactin–KD cells showed similar exponential loss of actin fluorescence ($t_{1/2}$ = 15.6 s) compared with DMSO-treated control cells. Importantly, the delayed actin turnover observed in YM201636-treated control cells was not observed in cortactin–KD cells with curve fits yielding $t_{1/2}$ of 15.5 s. These data indicate that PI(3,5)P_2 controls endosomal actin turnover in a cortactin-dependent manner.

PI(3,5)P_2 regulates actin assembly in cells with varying cortactin expression levels

As cortactin is frequently overexpressed in cancer cells, it is possible that excess cortactin might counteract the ability of PI(3,5)P_2 to remove it from endosomal actin. Our image analysis of PI(3,5)P_2 localization indicates that PI(3,5)P_2 is localized specifically to a subset of endosomal membranes (Fig. 2, B and C). Thresholding of those images allows us to estimate that ∼2.7% of the total cell area is occupied by PI(3,5)P_2, whereas cortactin is present throughout the entire cytoplasm, and thus has access to ∼66% of the total cell area. Using radioactive labeling with ^{3}[H]-inositol and HPLC analysis of phosphoinositide levels in MDA-MB-231 cells, we calculated a ratio of the PI(3,5)P_2+PI(3,4)P_2 peak to the PI(4,5)P_2 peak of 0.85% (Fig. S4, A–D). This represents a maximum ratio of PI(3,5)P_2 as it cannot be separated from PI(3,4)P_2 by HPLC, and is close to the ratio of PI(3,5)P_2 to PI(4,5)P_2 of 0.8% calculated in fibroblasts (Zolov et al., 2012). Using a previous estimate of the absolute concentration of PI(4,5)P_2 in cells to be 10 µM (McLaughlin et al., 2002), we estimate that the whole-cell level of PI(3,5)P_2 is up to 85 nM and that the concentration on endosomes could be 3.1 µM, based on our thresholding. We further estimated from Western blot analysis of cortactin levels in MDA-MB-231 cells (Fig. S4, E and F, 11.2 femtogram/cell), and using an approximate value for cell volume to be 4,190 µm^3 (McLaughlin et al., 2002), that the effective concentration of cortactin in cells is ∼67 nM. Thus, at late endosomes, we estimate that the concentration of PI(3,5)P_2 is 46-fold that of the concentration of cortactin molecules. This is a very rough estimate, as it does not take into account what fraction of cortactin is available to interact with PI(3,5)P_2 or local actin filament networks or what other effector molecules of PI(3,5)P_2 may be locally available to bind to PI(3,5)P_2. Nonetheless, it suggests that PI(3,5)P_2 is present at a high enough concentration at endosomes to effectively compete with actin filaments for cortactin binding across a range of cortactin concentrations. Furthermore, cortactin is unlikely to prevent the binding of other PI(3,5)P_2 effector molecules.

To specifically determine whether regulation of endosomal actin by PI(3,5)P_2 still occurs in cells overexpressing cortactin, we exogenously expressed cortactin using lentiviral transduction in MDA-MB-231 cells. In all cell lines, YM201636 treatment led to a large increase in cortactin and actin accumulation at late endosomes (Fig. S5). There was no effect of cortactin overexpression on the cortactin or actin colocalization with Rab7 in the absence of drug treatment. However, in the presence of YM201636, several of the cortactin-overexpressing

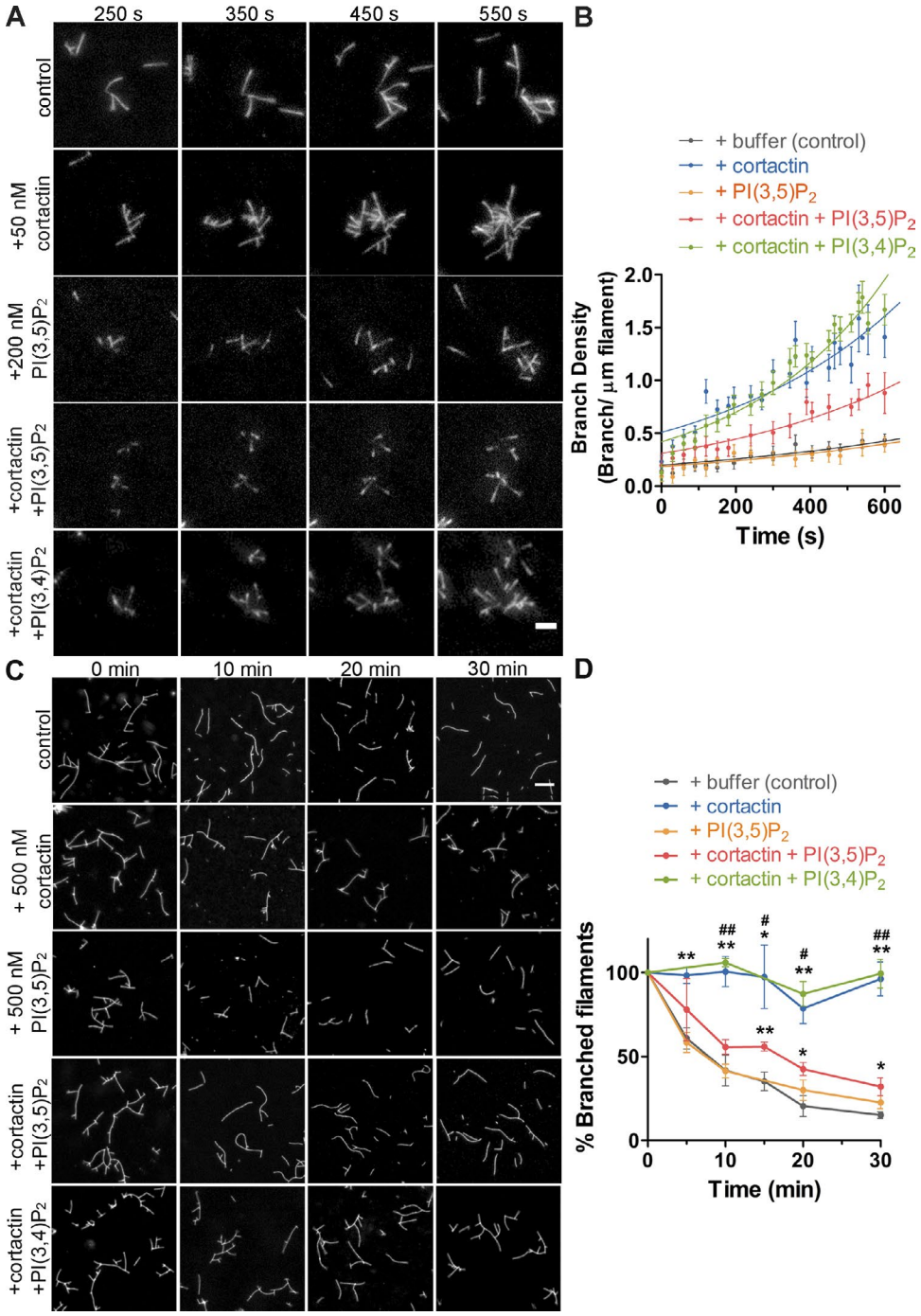

Figure 6. **PI(3,5)P_2 antagonizes the activity of cortactin in branched actin regulation.** (A and B) Synergistic activation of actin branching. (A) TIRF microscopy images of reactions containing actin (0.75 µM 33% Oregon Green labeled), 10 nM Arp2/3 complex, 50 nM GST-VCA, and the indicated amounts of cortactin and PI(3,5)P_2- or PI(3,4)P_2-liposomes. Bar, 3 µm. (B) Branch density plotted as a function of time. Error bars = SEM for ≥3 independent experiments. Branch density of cortactin + PI(3,5)P_2-liposomes was significantly decreased ($P < 0.05$) as compared with that of the +cortactin only condition for each time point after 150 s, except for the 390- and 450-s time points. (C) and (D) Debranching. (C) Representative images of actin debranching over time. 3 µM G-actin was polymerized in the presence of 100 nM Arp2/3 and 600 nM GST-VCA for 8 min. At that time, buffer, 500 nM cortactin, 500 nM PI(3,5)P_2, 500 nM cortactin + 500 nM PI(3,5)P_2-liposomes, or 500 nM cortactin + 500 nM PI(3,4)P_2-liposomes were added to individual reactions. Samples were incubated for an additional minute, as indicated, before the debranching reactions were stopped with 3 µM rhodamine-phalloidin and visualized. Bar, 3 µm. (D) Data points show percent branched filaments per field, calculated from three or four independent experiments. Error bars = SEM. * or #, $P < 0.05$; ** or ##, $P < 0.01$. Asterisks compare cortactin versus +buffer control and the # symbol compares +cortactin versus +cortactin + PI(3,5)P_2 condition.

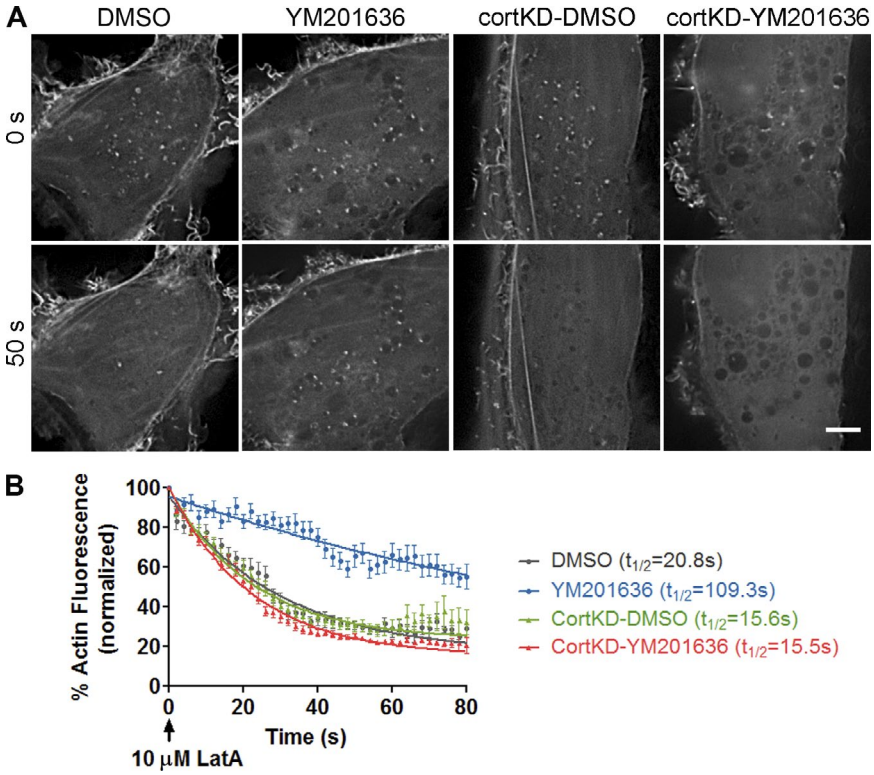

Figure 7. **Actin stability on endosomal membrane is controlled by PI(3,5)P_2.** MDA-MB-231 cells stably expressing mGFP-F-tractin were treated with DMSO or YM201636 for 2 h, and then imaged live after treatment with 10 µM latrunculin A (LatA). (A) Representative images at 0 and 50 s after LatA treatment. Bar, 5 µm. (B) The change in endosomal actin fluorescence over time after LatA treatment was normalized to initial endosomal actin fluorescence. *n* = 10–15 cells from 3 independent experiments for each condition.

cell lines had increased accumulation of actin and cortactin at late endosomes compared with control cells, suggesting that cortactin overexpression does affect endosomal actin. Importantly, these data indicate that PI(3,5)P_2 synthesis is able to control cortactin and actin accumulation at late endosomes across a range of cortactin concentrations.

WASH localization is regulated by PI(3,5)P_2

Activation of Arp2/3 complex occurs upon binding of an activator in the WASP family of proteins (Millard et al., 2004). At endosomes, the WASP family member WASH appears to be the main activator of Arp2/3 complex (Derivery et al., 2009; Gomez and Billadeau, 2009; Duleh and Welch, 2010) and should act in concert with cortactin to promote endosomal branched actin assembly. Consistent with those studies, WASH, cortactin, and actin show strong colocalization on endosomal membranes (Fig. 8). The FAM21 component of WASH has been found to bind multiple phosphoinositides by dot plot, including the major endosomal lipids PI(3)P and PI(3,5)P_2 (Jia et al., 2010). However, the consequence of that interaction is unclear. To assess the effect of PI(3,5)P_2 on WASH localization, MDA-MB-231 and SCC61 cells were treated with YM201636 and immunostained for WASH and cortactin and colocalized with either actin (Fig. 8 A) or mRFP-Rab7 (Fig. 8 B). Inhibition of PI(3,5)P_2 synthesis led to an increase in the localization of WASH to cortactin$^+$ and actin$^+$ structures at Rab7$^+$ endosomes (Fig. 8), suggesting that similarly to cortactin, PI(3,5)P_2 does not recruit WASH to endosomal membranes but instead may promote its removal. However, the increase in WASH localization to Rab7$^+$ endosomes was small compared with the increase in cortactin localization in YM201636-treated cells (40% increase in WASH vs. 300% increase in cortactin colocalization with Rab7, compare median values in Figs. 8 C and 3 C). As with endogenous Rab7 (Fig. 3 E), there was no difference in mRFP-Rab7 area with YM201636 treatment (Fig. 8 D). Overall, PI(3,5)P_2 plays a concerted role to remove branched actin regulators from late endosomes and promote disassembly of endosome-associated actin assemblies via cortactin (see model in Fig. 9).

Discussion

Dynamic actin assembly plays an important role in controlling cellular membrane trafficking. Here, we identify a specific molecular mechanism that regulates actin dynamics on endosomes: PI(3,5)P_2-mediated removal of cortactin from actin filament arrays. In vitro biochemical studies revealed that cortactin preferentially and specifically binds to PI(3,5)P_2 via its F-actin binding region. Furthermore, PI(3,5)P_2 inhibits binding of actin filaments to cortactin, as well as the activity of cortactin in branched actin assembly and stabilization. In cells, inhibition of PI(3,5)P_2 synthesis leads to accumulation of stable WASH–cortactin–actin assemblies on Rab7$^+$ endosomes. Finally, the accumulation of actin that occurs in the absence of PI(3,5)P_2 depends on the presence of cortactin, indicating a key role for PI(3,5)P_2–cortactin interactions in promoting turnover of late endosomal branched actin assemblies. These findings suggest a model in which actin dynamics on late endosomes are regulated by PI(3,5)P_2-induced cycling of cortactin on and off of actin filaments (see model in Fig. 9).

In cells, branched actin is very dynamic and controls rapid membrane events, including plasma membrane protrusions and membrane trafficking events. Our data indicate that the PI(3,5)P_2–cortactin interaction we described is a major regulator of actin dynamics at the late endosome and provide a unique example of coordination of endosomal actin dynamics. Because we did not detect significant binding of cortactin to other PIs, it is possible that this specific mechanism of PI–cort-

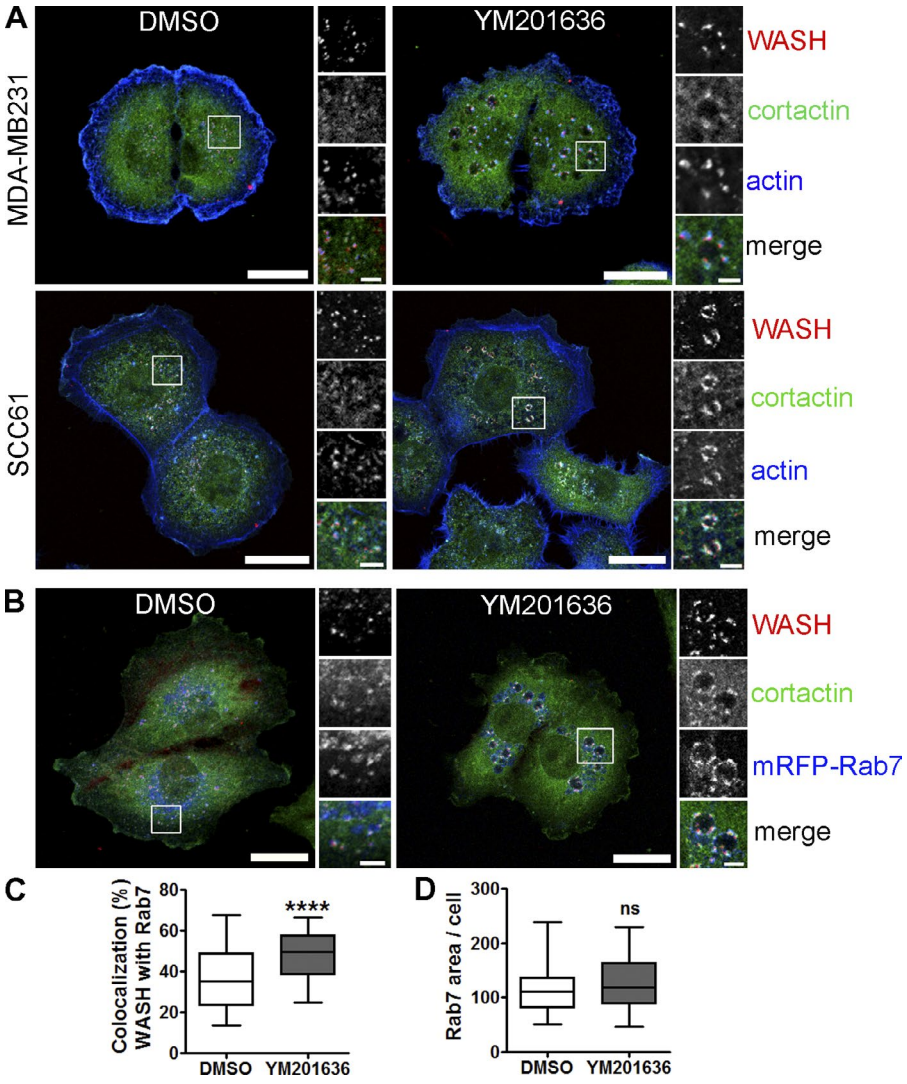

Figure 8. **WASH localization is controlled by PI(3,5)P_2 levels.** (A) Representative images from MDA-MB-231 (top) and SCC61 (bottom) showing localization of WASH (red), cortactin (green), and actin (blue) after 2-h treatment with 800 nM YM201636 or DMSO diluent control. Bars, 20 µm. (B) Representative images of MDA-MB-231 cells stably expressing mRFP-Rab7 (pseudocolored blue) immunostained by WASH (red) and cortactin (green) after 2-h treatment with 800 nM YM201636 or DMSO diluent control. Bars, 20 µm (5 µm for magnifications). (C and D) Images were analyzed for percentage of colocalization of WASH with Rab7 (C) and Rab7 area/cell (D). 2 independent experiments, $n \geq 62$ cells in each condition. ****, $P < 0.0001$.

actin interactions may be unique to the late endosome. At the plasma membrane, other mechanisms may control branched actin dynamics, including control of WAVE2-mediated actin polymerization by PI(3,4,5)P_3 (Oikawa et al., 2004). In addition, disassembly of lamellipodial branched actin networks may rely on other molecular mechanisms that promote debranching such as antagonism of cortactin by coronin and of antagonism of Arp2/3 complex by glial maturation factor (Cai et al., 2008; Gandhi et al., 2010; Luan and Nolen, 2013; Ydenberg et al., 2013). Endosomal actin turnover is also likely to be controlled by actin severing factors such as cofilin. Although we cannot rule out a role for such factors in PI(3,5)P_2-mediated regulation of actin stability, inhibition of PI(3,5)P_2 synthesis by YM201636 did not lead to any significant changes in cofilin activity as assessed by phosphorylation of the regulatory serine 3 of cofilin by Western blot analysis (Fig. S2 F). Conversely, inhibition of Arp2/3 complex or KD of cortactin did reverse the endosomal actin that accumulates with YM201636 treatment, indicating specific regulation of branched actin by PI(3,5)P_2.

Cortactin can promote actin assembly by both enhancing the ability of WASP family members to activate Arp2/3 complex and by stabilizing actin branches after they are formed (Weaver et al., 2001). Both of those activities require binding of cortactin to actin filaments and were inhibited by PI(3,5)P_2 binding in vitro. Because access to PI(3,5)P_2 is intrinsically limited to the membrane surface where WASH also is localized, a possible consequence of PI(3,5)P_2 binding to cortactin could be to limit coactivation of Arp2/3 complex. This mechanism would be consistent with the strong colocalization of WASH and cortactin on the endosome surface (Fig. 8) and is supported by in vitro evidence that cortactin and WASP family members uniquely act together to promote Arp2/3 complex activation (Weaver et al., 2001; Siton et al., 2011; Helgeson and Nolen, 2013). However, our finding that PI(3,5)P_2–cortactin interactions specifically promote turnover of endosomal actin in the absence of new actin polymerization (Fig. 7) suggests that inhibition of debranching is a key cortactin activity that is controlled by PI(3,5)P_2. Furthermore, inhibition of Arp2/3 complex but not PI(3,5)P_2 synthesis (Fig. 4) inhibited accumulation of cortactin at late endosomes. These data suggest a model in which activation of Arp2/3 complex leads to recruitment of cortactin to actin nucleation sites at the late endosome surface. Local synthesis of PI(3,5)P_2 would then promote removal of cortactin and net disassembly of endosomal actin (Fig. 9). Interestingly, the apparent K_d of 30 nM that we measured for cortactin–PI(3,5)P_2 interactions in pull-down assays is similar to the K_d of 17 nM recently measured for cortactin–branchpoint binding in live TIRF movies (Helgeson and Nolen, 2013).

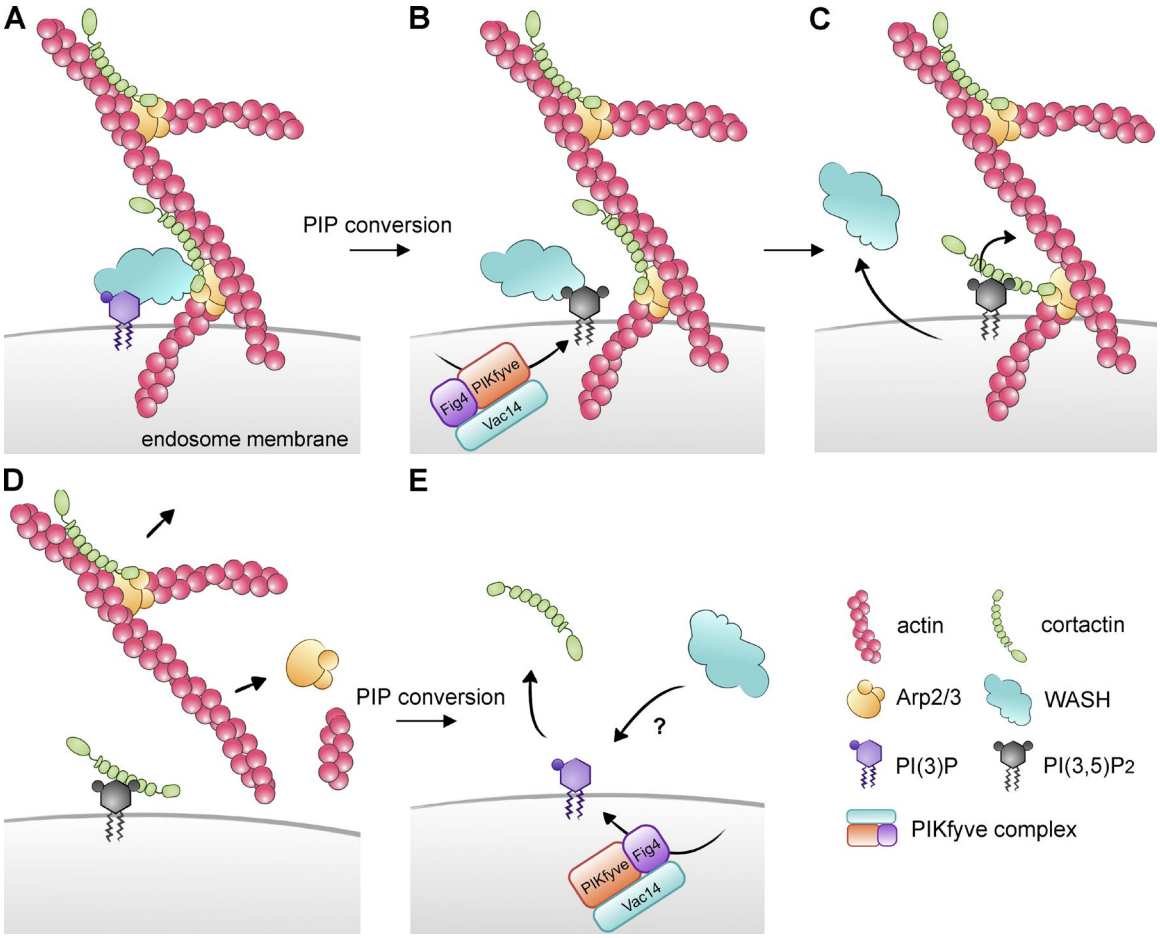

Figure 9. **Model of endosomal branched actin network regulation by PI(3,5)P_2.** (A) Branched actin nucleation is initiated by the WASH complex which is bound to the surface of late endosomes by signaling molecules that likely include PI(3)P (Jia et al., 2010). WASH-induced activation of the Arp2/3 complex recruits cortactin to nascent branch points (Fig. 4), where it synergistically promotes actin assembly. (B) Conversion of PI(3)P to PI(3,5)P_2 is accomplished by the enzymatic activity of PIKfyve within the three-member PIKfyve complex that includes the scaffold protein Vac14 and the opposing 5′ phosphatase Fig. 4 (Shisheva, 2008; Dove et al., 2009). (C) PI(3,5)P_2 binds to cortactin, releasing actin filaments (Fig. 5) and potentially the WASH complex from endosomes (Fig. 8). (D) Without cortactin binding to the branchpoint, Arp2/3 complex loses affinity for the mother filament (Uruno et al., 2001) causing debranching (Weaver et al., 2001; Fig. 6). Disassembly of branched actin networks leads to diminished recruitment of cortactin. (E) Conversion of PI(3,5)P_2 back to PI(3)P should release cortactin from the endosome surface unless new branched actin networks are available for rebinding. Interconversion of PI(3)P and PI(3,5)P_2 by the PIKfyve complex may facilitate dynamic cycling of actin assembly and disassembly through control of cortactin–actin interactions.

In addition to controlling cortactin localization to endosomes, inhibition of PI(3,5)P_2 synthesis led to a small but significant increase in WASH localization. Based on a previous study showing that WASH can bind the endosomal lipid PI(3)P (Jia et al., 2010), we speculate that conversion of PI(3)P to PI(3,5)P_2 could lead to loss of WASH from the endosomal surface (see Fig. 9 for model). However, to test this hypothesis, a detailed study of WASH–PIP binding using liposomes, as well as cellular experiments, would be required. It is also possible that PI(3,5)P_2 synthesis could indirectly lead to reduced WASH binding, by controlling the recruitment or activity of another WASH-binding partner. Nonetheless, it appears that PI(3,5)P_2 synthesis has a coordinate effect on both WASH and cortactin localization to late endosomes.

PI(3,5)P_2 regulates maturation of and trafficking from late endosomes. Our previous studies with cortactin–KD cells identified several strong phenotypes that are similar to those in cells with defective PI(3,5)P_2 formation, including enlargement of immature late endosomal/lysosomal compartments and defects in retrograde trafficking from late endosomes to the Golgi apparatus (Sung et al., 2011; Kirkbride et al., 2012). Moreover, cortactin-mediated actin remodeling is also known to regulate EGFR recycling and degradation in lysosomes (Timpson et al., 2005; Lladó et al., 2008) and autophagosome–lysosome fusion (Lee et al., 2010), both phenotypes controlled by PI(3,5)P_2 (de Lartigue et al., 2009). Notably, both overly stable and overly dynamic actin, as occurs, respectively with inhibition of PI(3,5)P_2 synthesis and cortactin–KD (Fig. 7), is associated with similar vacuolation and defective endosomal maturation phenotypes (de Lartigue et al., 2009; Kirkbride et al., 2012). These data suggest that actin dynamics must be finely tuned at late endosomes for proper maturation and functioning. Furthermore, our data suggest that control of branched actin dynamics through cortactin is at least one important mechanism by which PI(3,5)P_2 controls endosomal function.

In summary, we described a unique molecular mechanism that controls branched actin dynamics at late endosomes via PI(3,5)P_2-mediated removal of cortactin from actin filament networks. Dynamic cycling of phosphoinositides to orchestrate both assembly and disassembly of filament networks may be

a powerful mechanism to control actin–membrane interactions and downstream membrane-trafficking events.

Materials and methods

Plasmids and sequences

pEGFP-Vac14 controlled by the CMV promoter was generated by subcloning human Vac14 from pmCitrine-Vac14 (a gift from L. Wiesman, University of Michigan, Ann Arbor, MI) flanked with BgIII and Sal I sites into pEGFP-N1 (Takara Bio Inc.). pEGFP-mWASH encoding mouse WASH in pEGFP-C1 vector and controlled by the CMV promoter was a gift from L. Machesky (The Beatson Institute, Glasgow, Scotland, UK). pmCherry-ML1N*2 encoding N-terminal segment (residues 1–68) of the mouse TRPML1 and controlled by the CMV promoter was a gift from H. Xu (University of Michigan, Ann Arbor, MI). mGFP-F-tractin controlled by CMV promoter was a gift from R. Fischer (National Heart, Lung, and Blood Institute, National Institutes of Health [NIH], Bethesda, MD) and was created by cloning the 9–52 stretch of the F-actin–binding protein ITPKA into pCMVTag2A-mGFP. Human mRFP-Rab7 controlled by the CMV promoter was a gift from S. Pasternak (University of Western Ontario, London, Ontario, Canada). The lysine-to-glutamine mutations were introduced into the WT cortactin using the QuickChange II XL site-directed mutagenesis kit (Stratagene). All sequences were verified by DNA sequencing. Human mRFP-Rab7 was cloned into lentiviral, CMV-driven expression vectors using LR clonase (Gateway system; Invitrogen) between pENTR/SD/D-TOPO and pLenti6/V5-DEST. The 19-nt 552–570 of human cortactin, 5′-GCACGAGTCACAGAGAGAT-3′ was targeted for cortactin stable knockdown. PIKfyve knockdown was performed with an ON-TARGETplus siRNA SMARTpool (L-005058-00-0005; GE Dharmacon) using Lipofectamine RNAiMAX (Life Technologies). As a control for the knockdown, a nontargeting control pool was used (D-001810-10-05; GE Dharmacon).

Antibodies and reagents

Antibodies were as follows: mouse anti-cortactin (clone 4F11; Millipore), rabbit anti-Rab7 (#9367; BD), rabbit anti-GST antibody (#2622; Cell Signaling Technology), rhodamine-phalloidin (Molecular Probes), mouse anti-PIK5KIII (sc-100408; Santa Cruz Biotechnology, Inc.), rabbit anti-cofilin/phospho-cofilin (#5175/#3313; Cell Signaling Technology). Rabbit antisera to WASH was a gift from D. Billadeau (Mayo Clinic, Rochester, MN; Gomez and Billadeau, 2009) and was generated by immunizing rabbits with GST fusion WASH-VCA (aa 316–468; containing S324P, V386M, and G430R, as compared with BC048328). Rabbit anti-Arp2 antibody was a gift from M. Welch (University of California, Berkeley, Berkeley, CA; Gournier et al., 2001) and was obtained by immunizing rabbits with the synthetic peptide CKTLESSIQGLRIM followed by affinity purification. PIP strips and polyPIPosomes were from Echelon Biosciences (Y-P003, Y-P005, Y-P034, and Y-P035). All liposome experiments in the paper used polyPIPosomes. Latrunculin A was purchased from Sigma-Aldrich. YM201636 (Selleckchem), Apilimod (Axon Medchem), and CK-666 (Millipore) were stored as 10, 25, and 100 mM, respectively, stock solutions in DMSO. Purified Arp2/3 and labeled actin used in actin TIRF assay were a gift from J. Winkelman and D. Kovar (University of Chicago, Chicago, IL).

Cell culture and generation of stable cell line

MDA-MB-231 cells were maintained in DMEM supplemented with 10% FBS. SCC61 cells were maintained in DMEM supplemented with 20% FBS, 0.4 µg/ml hydrocortisone. HeLa cells were maintained in RPMI supplemented with 10% bovine growth serum (BGS). All cells were maintained at 37°C in 5% CO_2. Stable knockdown of cortactin or stable expression of mRFP-Rab7 was achieved using BLOCK-it Lentiviral RNAi expression system and ViralPower Lentiviral expression system (Invitrogen) according to the manufacturer's protocol.

Transfection and drug treatment

For mRFP-Rab7, mGFP-F-tractin, and EGFP-Vac14 mCherry-ML1N*2 transient transfections, cells were transfected with 0.5 µg/well of cDNA with Lipofectamine 3000. For inhibition of PIKfyve and Arp2/3 activity, cells grown on coverslips were serum starved (complete growth media lacking FBS) for 3 h before treating with YM201636, Apilimod, or CK-666, as previously described (Ikonomov et al., 2009). YM201636, Apilimod, and CK-666 dissolved in DMSO were diluted with DMEM and added to cells at a final concentration of 800 nM, 1 µM, and 100 µM, respectively, for 2 h.

For PIKfyve knockdown, cells were seeded in 6-well plates at a density of 2.0×10^5 cells/well before transfection using Lipofectamine RNAiMAX (Life Technologies) and 40 nM siRNA. After a 48-h incubation, cells were reseeded onto 6-well plates at the same density or onto coverslips at a density of 3.5×10^4 cells/well and retransfected with 40 nM oligos for 24 h. Cells were then processed for Western blotting and immunofluorescence.

Protein purification

To purify GST-tagged proteins, *Escherichia coli* BL21DE3 were transformed with the appropriate plasmid. After growth to approximately $OD_{600} = 0.8$, expression was induced with 1 mM IPTG for 20 h at 20°C. Cells were pelleted and resuspended in preparation buffer (300 mM NaCl, 0.5 mM EDTA, 50 mM Tris, pH 8.0) supplemented with 2 mg/ml lysozyme and protease inhibitors, and lysed with sonication. The lysate was then centrifuged at 96,000 *g* at 4°C for 30 min. The supernatant was incubated overnight with glutathione–Sepharose at 4°C before elution with 25 mM glutathione, 150 mM NaCl, 50 mM Tris, pH 8.0. Purified proteins were aliquoted, snap frozen in liquid nitrogen, and stored at –80°C. Actin was purified from chicken pectoralis skeletal muscle and gel filtered as described in (Bryce et al., 2005). In brief, chicken muscle acetone powder was thawed and mixed in G-buffer containing 2 mM Tris, pH 8.0, 0.2 mM ATP, 0.5 mM DTT, 0.005% NaN_3, and 0.2 mM $CaCl_2$. The supernatant was collected by centrifugation at 16,000 rpm at 4°C for 30 min and filtered through glass wool before mixing with 50 mM KCl and 2 mM $MgCl_2$ at 4°C for 1 h to polymerize the actin. KCl was added to make the supernatant 0.8 M KCl to dissociate tropomyosin, and then ultracentrifuged at 38,000 rpm for 2 h. Pellets were resuspended in G-buffer, homogenized, and dialyzed overnight to depolymerize actin. Actin monomers were gel filtered by passing through a Superdex 200 column. Actin-containing fractions were collected, snap frozen in liquid nitrogen, and stored at −80°C.

Lipid overlay assay

PIP strips were blocked in PBST (0.1% Tween 20 [vol/vol]) supplemented with 3% fatty acid-free BSA (Sigma-Aldrich) overnight at 4°C and then incubated with 0.5 µg/ml GST fusion proteins for 1 h at room temperature. After washes with PBST-BSA, the membranes were blotted with rabbit anti-GST for 1 h at room temperature, followed by IRDye 800 goat anti–rabbit secondary antibody for 1 h.

Liposome binding assay

For most experiments, 0.5 µg of purified GST fusion protein was incubated with 3 µM biotinylated liposomes composed of 5% PIP lipids in 20 mM Hepes, 120 mM NaCl, 1 mM EGTA, 0.2 mM $CaCl_2$, 1 mM $MgCl_2$, 5 mM KCl, and 1 mg/ml fatty acid-free BSA, pH 7.4, for 15 min at room temperature. For the binding isotherm (Fig. 1 D) and com-

petition assays (Fig. 5, E and F), 70 nM cortactin was used instead of 0.5 µg. Liposome–protein complexes were then further incubated with streptavidin-conjugated magnetic beads (Invitrogen) for 30 min at room temperature. After washing with binding buffer and isolation with a magnet, liposome-bound protein was analyzed by SDS-PAGE. The intensity of bands was quantified by ImageJ software (NIH). To compare relative binding affinity of each protein to $PI(3,5)P_2$, nonspecific bead binding band intensity (beads only lane) was subtracted from the specific liposome-bead band intensity, and then normalized by the intensity of the band in the input lane. Apparent equilibrium K_d were calculated using a one-site binding hyperbola nonlinear regression analysis in Prism (GraphPad, version 5 software).

Arp2/3 complex-binding assay

Purified GST or GST-fusion cortactin variants immobilized on glutathione beads, were incubated with 100 nM Arp2/3 complex in the binding buffer containing 20 mM Hepes, 60 mM KCl, 2 mM $MgCl_2$, 5 mg/ml BSA, pH 7.4, for 10 min at room temperature. Beads were washed three times with binding buffer, and bound proteins were eluted from the beads by boiling in SDS-PAGE loading buffer. Bound Arp2/3 complex was detected by Western blotting with anti-Arp2 polyclonal antibody.

F-actin co-sedimentation assay

F-actin was prepared from monomers by polymerization in 80 mM KCl, 2 mM $MgCl_2$, 20 mM Hepes, pH 7.4, for 1 h at room temperature. Next, 70 nM purified WT or mutant cortactin were incubated with 3 µM F-actin in polymerization buffer. After 10 min at room temperature, cortactin bound to actin filaments was separated from free cortactin by ultracentrifugation for 20 min at 175,000 *g*. Next, the supernatant and pellet fractions were analyzed by Western blotting using anti-GST antibody.

$PI(3,5)P_2$-F-actin competition assay

3 µM F-actin was prepared from monomers by polymerization in 80 mM KCl, 2 mM $MgCl_2$, and 20 mM Hepes, pH 7.4 for 1 h at room temperature. Next, various concentrations of actin filaments (0–1.5 µM) prepared by dilution with polymerization buffer were incubated with 250 nM $PI(3,5)P_2$-containing liposomes and 70 nM cortactin and then processed as for the liposome binding assay. GraphPad software was used for nonlinear regression analysis of datasets, and K_i was calculated using one-phase exponential decay equation.

Actin TIRF assay

Glass flow chambers were constructed from glass coverslips (24 × 40 mm and 22 × 22 mm; no. 1.5) using doubled-sided tape (3M). Coverslips were cleaned for 10 min with plasma cleaner and 30 min bath in 0.1 M KOH, and then coated with methoxy-polyethylene glycol-silane (mPEG-Silane-5K, Creative PEGworks; 0.1% in 95% ethanol, 0.1% HCl) overnight at room temperature. The mPEG-Silane coating was used to minimize filament binding to the chamber surface. The chambers were washed twice each with high then low salt buffer solutions (1% [wt/vol] BSA, 50 mM Tris, pH 7.5, and 600/150 mM NaCl, respectively), followed by two washes with 1× TIRF buffer. The 1× TIRF buffer contained MKEI (100 mM KCl, 2 mM $MgCl_2$, 2 mM EGTA, 20 mM imidazole, pH 7.0), 15 mM glucose, 100 mM DTT, 0.2 mM ATP, 0.5% 4000 cP methylcellulose, 20 µg/ml catalase, 0.1 mg/ml glucose oxidase, and 0.1% BSA. Glucose oxidase, catalase, and BSA were added just before use. Actin polymerization reactions were initiated by adding a protein solution containing the proteins (Arp2/3 complex, GST-VCA, cortactin, or $PI(3,5)P_2$-liposome) in 1× TIRF buffer to a solution of 4.5 µM 33% Oregon Green actin mixed with 50 µM $MgCl_2$ and 200 µM EGTA to give a final reaction solution of 0.75 µM 33% Oregon Green actin. Images were collected on a TiE inverted microscope (Nikon) equipped with a 100×/1.49 NA TIRF objective (Nikon), and Evolve EM-CCD camera (Photometrics). The 1.5× optivar was used for all images except for $PI(3,4)P_2$ condition (1×) to increase magnification. A 488-nm laser was used to excite Oregon Green. Images were acquired with Elements software (Nikon).

Debranching assay

Polymerization reactions were initiated by mixing 3 µM G-actin with 100 nM Arp2/3 complex and 600 nM GST-VCA in polymerization buffer, and incubated for 8 min to form fully polymerized actin branches. At this time, rhodamine-phalloidin (0 min sample), 500 nM cortactin, 500 nM cortactin plus 500 nM $PI(3,5)P_2$-liposome, 500 nM cortactin plus 500 nM $PI(3,4)P_2$-liposome, or buffer was added, then further incubated for 5, 10, 15, 20, or 30 min before adding equimolar (3 µM final concentration) rhodamine-phalloidin (from a 200 µM stock in methanol) to stop filament debranching and stain the actin filaments. After 4 min of incubation with rhodamine-phalloidin, filaments were diluted into fluorescence buffer containing MKEI, 100 mM dithiothreitol, 20 µg/ml catalase, 100 µg/ml glucose oxidase, 3 mg/ml glucose, and 0.5% methylcellulose, 4000cp. 4 µl was applied to glass coverslips (22 × 22 mm, #1.5; Thermo Fisher Scientific). Image were acquired with an Eclipse TE2000-E widefield fluorescent microscope (Nikon) equipped with a Plan Apo 100×/1.4 NA, oil immersion lens (used in combination with x1.5 optivar), and a cooled charge-coupled device camera (Hamamatsu Photonics) using MetaMorph software. Branching was analyzed by manually counting unbranched filaments and number of branching of filaments with one or more branches. Percent branching was then calculated by the following equation: percentage of branched filaments = (number of branched filaments per field/number of total filaments) × 100.

Immunofluorescence and Image analysis

Cells were fixed for 15 min in 4% paraformaldehyde at 37°C and blocked and permeabilized with 5% normal goat serum containing 0.3% Triton X-100 for 1 h at room temperature. Primary antibodies diluted in PBS containing 1% BSA and 0.3% Triton X-100 were added to cells for staining overnight at 4°C, followed by secondary antibody incubation for 1 h at room temperature. Cells were then mounted on slides with Aqua Poly/Mount mounting media (Polyscience, Inc.). Images were acquired at room temperature using an LSM Image browser software on a confocal microscope (model LSM 510; Carl Zeiss), using a Plan-Apochromat 63×/1.4 oil DIC objective and Argon2, HeNe1, and HeNe2 laser. Colocalization and intensity of single-plane images were quantitated using measure colocalization plug-in of MetaMorph software after thresholding images to remove background.

Live cell imaging

For visualization of the dynamic effect of YM201636 on endosomes, MDA-MB-231 cells stably expressing mRFP-Rab7 were cultured on poly-D-Lysine-coated MatTek dishes overnight. Before imaging, they were serum starved in DMEM for 3 h, and then 800 nM YM201636 was added. 20 min after drug treatment, images were captured every 10 s for 75 min on a confocal microscope (model LSM 710; Carl Zeiss) using a 63×/1.40 Plan-Apochromat oil objective and Argon-488 and HeNe-561 laser under 5% CO_2 at 37°C. For the analysis the stability of actin on endosomes, MDA-MB-231 cells stably expressing mRFP-Rab7 were transfected with the actin probe mGFP-F-tractin. Next, cells were cultured on 35-mm glass bottom dishes (no. 1.5; In Vitro Scientific) overnight. After 2-h incubation of cells with DMSO or YM201636, 10 µM latrunculin A was added and images were captured every 2 s with SoftWoRx software on a DeltaVision deconvolution mi-

croscope (Applied Precision) equipped with a CoolSNAP HQ2 camera (Photometrics), and a UPSLAPO 100×/1.4 NA oil immersion objective. Individual raw files were deconvoluted using Applied Precision SoftWoRx deconvolution package. Fluorescence intensity of individual endosomal mGFP-F-tractin spots were tracked over time using the manual tracking plugin of Fiji software. Individual endosomal actin spots, adjacent cytosolic background, and background outside the cell were compared for each time point using this plugin to measure pixel intensities. For data plots, the background intensity outside of the cell was subtracted at each time point and the ratio of endosomal to cytosolic mGFP-F-tractin intensity was plotted. Data were fitted with a one-phase decay equation model using GraphPad Prism software to determine the half-life ($t_{1/2}$) of endosomal actin.

Analysis of PI lipids in cells

As a positive control, *Saccharomyces cerevisiae* (w303 strain) was grown in 2 ml complete synthetic medium with 30 µCi/ml ^{3}[H]-inositol (Perkin Elmer) overnight at 30°C to reach saturation. Half of the cultures were osmotically shocked by adding KCl (1M) for 10 min to induce PI(3,5)P_2 synthesis. Lipids from the harvested yeasts were extracted and deacylated (Bird, 1994). For MDA-MB-231 cells, 5 × 10^5 cells/60-mm dish were seeded and grown at 37°C overnight before washing with inositol-free DMEM-H medium (MP Biomedicals), and growing in 5 ml of inositol-free DMEM-H with 30 µCi/ml ^{3}[H]-inositol and 10% dialyzed FBS for 3 d to reach full confluence. Cellular lipids were then extracted and deacylated. The deacylated lipids were analyzed by HPLC on a Partisphere SAX column (4.6 × 125 mm; Whatman) using the following buffer profile: 10 mM $NH_4H_2PO_4$ (pH 3.5, buffer A) for 7 min, 0–7% buffer B (1.7 M $NH_4H_2PO_4$, pH 3.5) in the next 3 min, 7–14% buffer B in the next 15 min, then 14–60% buffer B for the next 10 min, and followed by 60–100% buffer B for another 15 min. The flow rate throughout the gradient was 1 ml/min, and 1-ml fractions from the column were quantified by scintillation counting.

Data graphing and statistical analysis

Graphs were generated using Prism GraphPad version 5. Statistical analysis was performed using SPSS version 22. All data were tested for normality using a Kolmogorov-Smirnov normality test. Data with a normal distribution were analyzed using a two-tailed Student's *t* test and plotted using mean + standard error bar graphs. Data with a nonnormal (nonparametric) distribution were analyzed using a Mann-Whitney *U* test and presented as box and whiskers plots with the box indicating the 25th and 75th percentiles, solid line indicating the median, and the whiskers indicating the 95% confidence intervals.

Online supplemental material

Fig. S1 shows analysis of purified proteins by SDS-PAGE and additional liposome pull-down data. Fig. S2 shows the effect of inhibition of PI(3,5)P_2 synthesis on endosomal actin, endosomal compartments, and cofilin phosphorylation. Fig. S3 shows the contribution of lysines in the cortactin fourth repeat domain to F-actin and PI(3,5)P_2 binding. Fig. S4 shows analysis and calculation of the cellular concentrations of PI(3,5)P_2 and cortactin. Fig. S5 shows that PI(3,5)P_2 regulates endosomal actin assembly in cells with varying cortactin overexpression levels. Video 1 shows the enlargement of Rab7$^+$ endosomes upon YM201636 treatment. Video 2 shows actin branching dynamics in control condition. Video 3 shows actin branching dynamics in the presence of cortactin. Video 4 shows actin branching dynamics in the presence of PI(3,5)P_2-liposomes. Video 5 shows actin branching dynamics in the presence of both cortactin and PI(3,5)P_2-liposomes. Video 6 shows actin branching dynamics in the presence of both cortactin and PI(3,4)P_2-liposomes. Video 7 shows changes in endosomal actin stability on Rab7$^+$ endosomes upon YM201636 treatment in control and cortactin–KD cells. Online supplemental material is available at http://www.jcb.org/cgi/content/full/jcb.201412127/DC1.

Acknowledgments

We thank Dr. Nelson Alexander for pilot data and critical reading of the manuscript. We thank Dr. David Kovar and Jon Winkelman for advice on actin TIRF imaging and purified proteins, Jessica Mazerik for advice on liposome assays, Dr. Matthew Tyska for use of the TIRF microscope and plasma cleaner and scientific feedback, Dr. John York for help with PIP lipid analysis, and Weaver laboratory members for scientific feedback.

Funding was provided by NIH grants R01CA163592 and R01GM075126 (A.M. Weaver), R01 HL-55672 (A. Qi), CTSA grants UL1 RR024975 and TR000445-06, grants supporting VUMC CISR CA68485, DK20593, DK58404, HD15052, DK59637, and EY08126. This publication's contents are solely the responsibility of the authors and do not necessarily represent the official views of the NIH.

The authors declare no competing financial interests.

Submitted: 26 December 2014
Accepted: 23 July 2015

References

Behnia, R., and S. Munro. 2005. Organelle identity and the signposts for membrane traffic. *Nature.* 438:597–604. http://dx.doi.org/10.1038/nature04397

Bird, I.M. 1994. Analysis of cellular phosphoinositides and phosphoinositols by extraction and simple analytical procedures. *Methods Mol. Biol.* 27:227–248.

Bolino, A., M. Muglia, F.L. Conforti, E. LeGuern, M.A. Salih, D.M. Georgiou, K. Christodoulou, I. Hausmanowa-Petrusewicz, P. Mandich, A. Schenone, et al. 2000. Charcot-Marie-Tooth type 4B is caused by mutations in the gene encoding myotubularin-related protein-2. *Nat. Genet.* 25:17–19. http://dx.doi.org/10.1038/75542

Bryce, N.S., E.S. Clark, J.L. Leysath, J.D. Currie, D.J. Webb, and A.M. Weaver. 2005. Cortactin promotes cell motility by enhancing lamellipodial persistence. *Curr. Biol.* 15:1276–1285. http://dx.doi.org/10.1016/j.cub.2005.06.043

Cai, L., A.M. Makhov, D.A. Schafer, and J.E. Bear. 2008. Coronin 1B antagonizes cortactin and remodels Arp2/3-containing actin branches in lamellipodia. *Cell.* 134:828–842. http://dx.doi.org/10.1016/j.cell.2008.06.054

Cai, X., Y. Xu, A.K. Cheung, R.C. Tomlinson, A. Alcázar-Román, L. Murphy, A. Billich, B. Zhang, Y. Feng, M. Klumpp, et al. 2013. PIKfyve, a class III PI kinase, is the target of the small molecular IL-12/IL-23 inhibitor apilimod and a player in Toll-like receptor signaling. *Chem. Biol.* 20:912–921. http://dx.doi.org/10.1016/j.chembiol.2013.05.010

Chow, C.Y., Y. Zhang, J.J. Dowling, N. Jin, M. Adamska, K. Shiga, K. Szigeti, M.E. Shy, J. Li, X. Zhang, et al. 2007. Mutation of FIG4 causes neurodegeneration in the pale tremor mouse and patients with CMT4J. *Nature.* 448:68–72. http://dx.doi.org/10.1038/nature05876

de Lartigue, J., H. Polson, M. Feldman, K. Shokat, S.A. Tooze, S. Urbé, and M.J. Clague. 2009. PIKfyve regulation of endosome-linked pathways. *Traffic.* 10:883–893. http://dx.doi.org/10.1111/j.1600-0854.2009.00915.x

Derivery, E., C. Sousa, J.J. Gautier, B. Lombard, D. Loew, and A. Gautreau. 2009. The Arp2/3 activator WASH controls the fission of endosomes through a large multiprotein complex. *Dev. Cell.* 17:712–723. http://dx.doi.org/10.1016/j.devcel.2009.09.010

Di Paolo, G., and P. De Camilli. 2006. Phosphoinositides in cell regulation and membrane dynamics. *Nature.* 443:651–657. http://dx.doi.org/10.1038/nature05185

Dove, S.K., K. Dong, T. Kobayashi, F.K. Williams, and R.H. Michell. 2009. Phosphatidylinositol 3,5-bisphosphate and Fab1p/PIKfyve underPPIn endo-lysosome function. *Biochem. J.* 419:1–13. http://dx.doi.org/10.1042/BJ20081950

Duleh, S.N., and M.D. Welch. 2010. WASH and the Arp2/3 complex regulate endosome shape and trafficking. *Cytoskeleton (Hoboken).* 67:193–206.

Ferguson, C.J., G.M. Lenk, and M.H. Meisler. 2009. Defective autophagy in neurons and astrocytes from mice deficient in PI(3,5)P_2. *Hum. Mol. Genet.* 18:4868–4878. http://dx.doi.org/10.1093/hmg/ddp460

Gandhi, M., B.A. Smith, M. Bovellan, V. Paavilainen, K. Daugherty-Clarke, J. Gelles, P. Lappalainen, and B.L. Goode. 2010. GMF is a cofilin homolog that binds Arp2/3 complex to stimulate filament debranching and inhibit actin nucleation. *Curr. Biol.* 20:861–867. http://dx.doi.org/10.1016/j.cub.2010.03.026

Goley, E.D., and M.D. Welch. 2006. The ARP2/3 complex: an actin nucleator comes of age. *Nat. Rev. Mol. Cell Biol.* 7:713–726. http://dx.doi.org/10.1038/nrm2026

Gomez, T.S., and D.D. Billadeau. 2009. A FAM21-containing WASH complex regulates retromer-dependent sorting. *Dev. Cell.* 17:699–711. http://dx.doi.org/10.1016/j.devcel.2009.09.009

Gournier, H., E.D. Goley, H. Niederstrasser, T. Trinh, and M.D. Welch. 2001. Reconstitution of human Arp2/3 complex reveals critical roles of individual subunits in complex structure and activity. *Mol. Cell.* 8:1041–1052. http://dx.doi.org/10.1016/S1097-2765(01)00393-8

He, H., T. Watanabe, X. Zhan, C. Huang, E. Schuuring, K. Fukami, T. Takenawa, C.C. Kumar, R.J. Simpson, and H. Maruta. 1998. Role of phosphatidylinositol 4,5-bisphosphate in Ras/Rac-induced disruption of the cortactin-actomyosin II complex and malignant transformation. *Mol. Cell. Biol.* 18:3829–3837.

Helgeson, L.A., and B.J. Nolen. 2013. Mechanism of synergistic activation of Arp2/3 complex by cortactin and N-WASP. *eLife.* 2:e00884. http://dx.doi.org/10.7554/eLife.00884

Helgeson, L.A., J.G. Prendergast, A.R. Wagner, M. Rodnick-Smith, and B.J. Nolen. 2014. Interactions with actin monomers, actin filaments, and Arp2/3 complex define the roles of WASP family proteins and cortactin in coordinately regulating branched actin networks. *J. Biol. Chem.* 289:28856–28869. http://dx.doi.org/10.1074/jbc.M114.587527

Hetrick, B., M.S. Han, L.A. Helgeson, and B.J. Nolen. 2013. Small molecules CK-666 and CK-869 inhibit actin-related protein 2/3 complex by blocking an activating conformational change. *Chem. Biol.* 20:701–712. http://dx.doi.org/10.1016/j.chembiol.2013.03.019

Ikonomov, O.C., D. Sbrissa, and A. Shisheva. 2006. Localized PtdIns 3,5-P_2 synthesis to regulate early endosome dynamics and fusion. *Am. J. Physiol. Cell Physiol.* 291:C393–C404. http://dx.doi.org/10.1152/ajpcell.00019.2006

Ikonomov, O.C., D. Sbrissa, and A. Shisheva. 2009. YM201636, an inhibitor of retroviral budding and PIKfyve-catalyzed PtdIns(3,5)P_2 synthesis, halts glucose entry by insulin in adipocytes. *Biochem. Biophys. Res. Commun.* 382:566–570. http://dx.doi.org/10.1016/j.bbrc.2009.03.063

Janmey, P.A., and U. Lindberg. 2004. Cytoskeletal regulation: rich in lipids. *Nat. Rev. Mol. Cell Biol.* 5:658–666. http://dx.doi.org/10.1038/nrm1434

Jefferies, H.B., F.T. Cooke, P. Jat, C. Boucheron, T. Koizumi, M. Hayakawa, H. Kaizawa, T. Ohishi, P. Workman, M.D. Waterfield, and P.J. Parker. 2008. A selective PIKfyve inhibitor blocks PtdIns(3,5)P(2) production and disrupts endomembrane transport and retroviral budding. *EMBO Rep.* 9:164–170. http://dx.doi.org/10.1038/sj.embor.7401155

Jia, D., T.S. Gomez, Z. Metlagel, J. Umetani, Z. Otwinowski, M.K. Rosen, and D.D. Billadeau. 2010. WASH and WAVE actin regulators of the Wiskott-Aldrich syndrome protein (WASP) family are controlled by analogous structurally related complexes. *Proc. Natl. Acad. Sci. USA.* 107:10442–10447. http://dx.doi.org/10.1073/pnas.0913293107

Jin, N., C.Y. Chow, L. Liu, S.N. Zolov, R. Bronson, M. Davisson, J.L. Petersen, Y. Zhang, S. Park, and J.E. Duexet al.. 2008. VAC14 nucleates a protein complex essential for the acute interconversion of PI3P and PI(3,5)P_2 in yeast and mouse. *EMBO J.* 27:3221–3234. http://dx.doi.org/10.1038/emboj.2008.248

Kirkbride, K.C., N.H. Hong, C.L. French, E.S. Clark, W.G. Jerome, and A.M. Weaver. 2012. Regulation of late endosomal/lysosomal maturation and trafficking by cortactin affects Golgi morphology. Cytoskeleton, Hoboken.

Kotoulas, A., H. Kokotas, K. Kopsidas, K. Droutsas, M. Grigoriadou, H. Bajrami, D.F. Schorderet, and M.B. Petersen. 2011. A novel PIKFYVE mutation in fleck corneal dystrophy. *Mol. Vis.* 17:2776–2781.

Kutateladze, T.G. 2010. Translation of the phosphoinositide code by PI effectors. *Nat. Chem. Biol.* 6:507–513. http://dx.doi.org/10.1038/nchembio.390

Lai, F.P., M. Szczodrak, J. Block, J. Faix, D. Breitsprecher, H.G. Mannherz, T.E. Stradal, G.A. Dunn, J.V. Small, and K. Rottner. 2008. Arp2/3 complex interactions and actin network turnover in lamellipodia. *EMBO J.* 27:982–992. http://dx.doi.org/10.1038/emboj.2008.34

Lee, J.Y., H. Koga, Y. Kawaguchi, W. Tang, E. Wong, Y.S. Gao, U.B. Pandey, S. Kaushik, E. Tresse, J. Lu, et al. 2010. HDAC6 controls autophagosome maturation essential for ubiquitin-selective quality-control autophagy. *EMBO J.* 29:969–980. http://dx.doi.org/10.1038/emboj.2009.405

Li, X., X. Wang, X. Zhang, M. Zhao, W.L. Tsang, Y. Zhang, R.G. Yau, L.S. Weisman, and H. Xu. 2013. Genetically encoded fluorescent probe to visualize intracellular phosphatidylinositol 3,5-bisphosphate localization and dynamics. *Proc. Natl. Acad. Sci. USA.* 110:21165–21170. http://dx.doi.org/10.1073/pnas.1311864110

Lladó, A., P. Timpson, S. Vilà de Muga, J. Moretó, A. Pol, T. Grewal, R.J. Daly, C. Enrich, and F. Tebar. 2008. Protein kinase Cdelta and calmodulin regulate epidermal growth factor receptor recycling from early endosomes through Arp2/3 complex and cortactin. *Mol. Biol. Cell.* 19:17–29. http://dx.doi.org/10.1091/mbc.E07-05-0411

Luan, Q., and B.J. Nolen. 2013. Structural basis for regulation of Arp2/3 complex by GMF. *Nat. Struct. Mol. Biol.* 20:1062–1068. http://dx.doi.org/10.1038/nsmb.2628

McLaughlin, S., J. Wang, A. Gambhir, and D. Murray. 2002. PIP(2) and proteins: interactions, organization, and information flow. *Annu. Rev. Biophys. Biomol. Struct.* 31:151–175. http://dx.doi.org/10.1146/annurev.biophys.31.082901.134259

Michell, R.H., V.L. Heath, M.A. Lemmon, and S.K. Dove. 2006. Phosphatidylinositol 3,5-bisphosphate: metabolism and cellular functions. *Trends Biochem. Sci.* 31:52–63. http://dx.doi.org/10.1016/j.tibs.2005.11.013

Millard, T.H., S.J. Sharp, and L.M. Machesky. 2004. Signalling to actin assembly via the WASP (Wiskott-Aldrich syndrome protein)-family proteins and the Arp2/3 complex. *Biochem. J.* 380:1–17. http://dx.doi.org/10.1042/BJ20040176

Monteiro, P., C. Rossé, A. Castro-Castro, M. Irondelle, E. Lagoutte, P. Paul-Gilloteaux, C. Desnos, E. Formstecher, F. Darchen, D. Perrais, et al. 2013. Endosomal WASH and exocyst complexes control exocytosis of MT1-MMP at invadopodia. *J. Cell Biol.* 203:1063–1079. http://dx.doi.org/10.1083/jcb.201306162

Morton, W.M., K.R. Ayscough, and P.J. McLaughlin. 2000. Latrunculin alters the actin-monomer subunit interface to prevent polymerization. *Nat. Cell Biol.* 2:376–378. http://dx.doi.org/10.1038/35014075

Nicot, A.S., H. Fares, B. Payrastre, A.D. Chisholm, M. Labouesse, and J. Laporte. 2006. The phosphoinositide kinase PIKfyve/Fab1p regulates terminal lysosome maturation in Caenorhabditis elegans. *Mol. Biol. Cell.* 17:3062–3074.

Nolen, B.J., N. Tomasevic, A. Russell, D.W. Pierce, Z. Jia, C.D. McCormick, J. Hartman, R. Sakowicz, and T.D. Pollard. 2009. Characterization of two classes of small molecule inhibitors of Arp2/3 complex. *Nature.* 460:1031–1034. http://dx.doi.org/10.1038/nature08231

Ohashi, E., K. Tanabe, Y. Henmi, K. Mesaki, Y. Kobayashi, and K. Takei. 2011. Receptor sorting within endosomal trafficking pathway is facilitated by dynamic actin filaments. *PLoS ONE.* 6:e19942. http://dx.doi.org/10.1371/journal.pone.0019942

Oikawa, T., H. Yamaguchi, T. Itoh, M. Kato, T. Ijuin, D. Yamazaki, S. Suetsugu, and T. Takenawa. 2004. PtdIns(3,4,5)P_3 binding is necessary for WAVE2-induced formation of lamellipodia. *Nat. Cell Biol.* 6:420–426. http://dx.doi.org/10.1038/ncb1125

Otomo, A., L. Pan, and S. Hadano. 2012. Dysregulation of the autophagy-endolysosomal system in amyotrophic lateral sclerosis and related motor neuron diseases. *Neurol. Res. Int.* 2012:498428. http://dx.doi.org/10.1155/2012/498428

Papayannopoulos, V., C. Co, K.E. Prehoda, S. Snapper, J. Taunton, and W.A. Lim. 2005. A polybasic motif allows N-WASP to act as a sensor of PIP(2) density. *Mol. Cell.* 17:181–191. http://dx.doi.org/10.1016/j.molcel.2004.11.054

Puthenveedu, M.A., B. Lauffer, P. Temkin, R. Vistein, P. Carlton, K. Thorn, J. Taunton, O.D. Weiner, R.G. Parton, and M. von Zastrow. 2010. Sequence-dependent sorting of recycling proteins by actin-stabilized endosomal microdomains. *Cell.* 143:761–773. http://dx.doi.org/10.1016/j.cell.2010.10.003

Rohatgi, R., H.Y. Ho, and M.W. Kirschner. 2000. Mechanism of N-WASP activation by CDC42 and phosphatidylinositol 4, 5-bisphosphate. *J. Cell Biol.* 150:1299–1310. http://dx.doi.org/10.1083/jcb.150.6.1299

Rossé, C., C. Lodillinsky, L. Fuhrmann, M. Nourieh, P. Monteiro, M. Irondelle, E. Lagoutte, S. Vacher, F. Waharte, P. Paul-Gilloteaux, et al. 2014. Control of MT1-MMP transport by atypical PKC during breast-cancer progression. *Proc. Natl. Acad. Sci. USA.* 111:E1872–E1879. http://dx.doi.org/10.1073/pnas.1400749111

Rudge, S.A., D.M. Anderson, and S.D. Emr. 2004. Vacuole size control: regulation of PtdIns(3,5)P2 levels by the vacuole-associated Vac14-Fig4 complex, a PtdIns(3,5)P2-specific phosphatase. *Mol. Biol. Cell.* 15:24–36. http://dx.doi.org/10.1091/mbc.E03-05-0297

Rusten, T.E., L.M. Rodahl, K. Pattni, C. Englund, C. Samakovlis, S. Dove, A. Brech, and H. Stenmark. 2006. Fab1 phosphatidylinositol 3-phos-

phate 5-kinase controls trafficking but not silencing of endocytosed receptors. *Mol. Biol. Cell.* 17:3989–4001. http://dx.doi.org/10.1091/mbc.E06-03-0239

Rutherford, A.C., C. Traer, T. Wassmer, K. Pattni, M.V. Bujny, J.G. Carlton, H. Stenmark, and P.J. Cullen. 2006. The mammalian phosphatidylinositol 3-phosphate 5-kinase (PIKfyve) regulates endosome-to-TGN retrograde transport. *J. Cell Sci.* 119:3944–3957. http://dx.doi.org/10.1242/jcs.03153

Saarikangas, J., H. Zhao, and P. Lappalainen. 2010. Regulation of the actin cytoskeleton-plasma membrane interplay by phosphoinositides. *Physiol. Rev.* 90:259–289. http://dx.doi.org/10.1152/physrev.00036.2009

Shisheva, A. 2008. PIKfyve: Partners, significance, debates and paradoxes. *Cell Biol. Int.* 32:591–604. http://dx.doi.org/10.1016/j.cellbi.2008.01.006

Siton, O., Y. Ideses, S. Albeck, T. Unger, A.D. Bershadsky, N.S. Gov, and A. Bernheim-Groswasser. 2011. Cortactin releases the brakes in actin-based motility by enhancing WASP-VCA detachment from Arp2/3 branches. *Curr. Biol.* 21:2092–2097. http://dx.doi.org/10.1016/j.cub.2011.11.010

Suetsugu, S., S. Kurisu, T. Oikawa, D. Yamazaki, A. Oda, and T. Takenawa. 2006. Optimization of WAVE2 complex-induced actin polymerization by membrane-bound IRSp53, PIP_3, and Rac. *J. Cell Biol.* 173:571–585. http://dx.doi.org/10.1083/jcb.200509067

Sung, B.H., X. Zhu, I. Kaverina, and A.M. Weaver. 2011. Cortactin controls cell motility and lamellipodial dynamics by regulating ECM secretion. *Curr. Biol.* 21:1460–1469. http://dx.doi.org/10.1016/j.cub.2011.06.065

Tanabe, K., E. Ohashi, Y. Henmi, and K. Takei. 2011. Receptor sorting and actin dynamics at early endosomes. *Commun. Integr. Biol.* 4:742–744. http://dx.doi.org/10.4161/cib.17628

Timpson, P., D.K. Lynch, D. Schramek, F. Walker, and R.J. Daly. 2005. Cortactin overexpression inhibits ligand-induced down-regulation of the epidermal growth factor receptor. *Cancer Res.* 65:3273–3280.

Uruno, T., J. Liu, P. Zhang, Y. Fan Yx, C. Egile, R. Li, S.C. Mueller, and X. Zhan. 2001. Activation of Arp2/3 complex-mediated actin polymerization by cortactin. *Nat. Cell Biol.* 3:259–266. http://dx.doi.org/10.1038/35060051

Uruno, T., J. Liu, Y. Li, N. Smith, and X. Zhan. 2003. Sequential interaction of actin-related proteins 2 and 3 (Arp2/3) complex with neural Wiscott-Aldrich syndrome protein (N-WASP) and cortactin during branched actin filament network formation. *J. Biol. Chem.* 278:26086–26093. http://dx.doi.org/10.1074/jbc.M301997200

van Rossum, A.G., J.H. de Graaf, E. Schuuring-Scholtes, P.M. Kluin, Y.X. Fan, X. Zhan, W.H. Moolenaar, and E. Schuuring. 2003. Alternative splicing of the actin binding domain of human cortactin affects cell migration. *J. Biol. Chem.* 278:45672–45679. http://dx.doi.org/10.1074/jbc.M306688200

Weaver, A.M., A.V. Karginov, A.W. Kinley, S.A. Weed, Y. Li, J.T. Parsons, and J.A. Cooper. 2001. Cortactin promotes and stabilizes Arp2/3-induced actin filament network formation. *Curr. Biol.* 11:370–374. http://dx.doi.org/10.1016/S0960-9822(01)00098-7

Weaver, A.M., J.E. Heuser, A.V. Karginov, W.L. Lee, J.T. Parsons, and J.A. Cooper. 2002. Interaction of cortactin and N-WASp with Arp2/3 complex. *Curr. Biol.* 12:1270–1278. http://dx.doi.org/10.1016/S0960-9822(02)01035-7

Weed, S.A., A.V. Karginov, D.A. Schafer, A.M. Weaver, A.W. Kinley, J.A. Cooper, and J.T. Parsons. 2000. Cortactin localization to sites of actin assembly in lamellipodia requires interactions with F-actin and the Arp2/3 complex. *J. Cell Biol.* 151:29–40.

Wu, H., A.B. Reynolds, S.B. Kanner, R.R. Vines, and J.T. Parsons. 1991. Identification and characterization of a novel cytoskeleton-associated pp60src substrate. *Mol. Cell. Biol.* 11:5113–5124.

Ydenberg, C.A., S.B. Padrick, M.O. Sweeney, M. Gandhi, O. Sokolova, and B.L. Goode. 2013. GMF severs actin-Arp2/3 complex branch junctions by a cofilin-like mechanism. *Curr. Biol.* 23:1037–1045. http://dx.doi.org/10.1016/j.cub.2013.04.058

Yin, H.L., and P.A. Janmey. 2003. Phosphoinositide regulation of the actin cytoskeleton. *Annu. Rev. Physiol.* 65:761–789. http://dx.doi.org/10.1146/annurev.physiol.65.092101.142517

Zolov, S.N., D. Bridges, Y. Zhang, W.W. Lee, E. Riehle, R. Verma, G.M. Lenk, K. Converso-Baran, T. Weide, and R.L. Albinet al.. 2012. In vivo, Pikfyve generates $PI(3,5)P_2$, which serves as both a signaling lipid and the major precursor for PI5P. *Proc. Natl. Acad. Sci. USA.* 109:17472–17477. http://dx.doi.org/10.1073/pnas.1203106109